國立臺灣大學理學院化學系

碩士論文

Department of Chemistry

College of Science

National Taiwan University

Master Thesis

非簡諧振動分析中振動座標的最佳化

Optimization of Coordinates for Anharmonic Vibrational Analysis

阮荷娟

Ha-Quyen Nguyen

指導教授: 鄭原忠 博士

Advisor: Yuan-Chung Cheng Ph.D.

中華民國 111 年 8 月

August, 2022

doi:10.6342/NTU202201978

國立臺灣大學碩士學位論
口試委員會審定書
NTU Master Thesis
Oral Defense Approval Form

（論文中文題目 Thesis Title in Chinese）非簡諧振動分析中振動座標的最佳化

（論文英文題目 Thesis Title in English）Optimization of Coordinates for Anharmonic Vibrational Analysis

本論文係阮荷娟君（學號R09223180）在國立臺灣大學化學系完成之碩士學位論文，於民國2022年07月15日承下列考試委員審查通過及口試及格，特此證明。

The student 阮荷娟 (student no. R09223180) enrolled in the Master Program of the Department of Chemistry, NTU has satisfactorily passed the oral defense on _____(date)_____ with the approval of all committee members as follows. 2022/07/15

口試委員(Committee Members)：

鄭原忠 （簽名 Signature）

（指導教授 Advisor）

林倫年

系主任、所長 梁文傑 （簽章）

(Dept./Institute Chair's Signature and Seal)

doi:10.6342/NTU202201978

doi:10.6342/NTU202201978

Acknowledgements

First of all, I would like to thank Prof. Yuan-Chung Cheng for taking me as a student in the Department of Chemistry. I would also like to thank Prof. Yuan-Chung Cheng, Dr. Jer-Lai Kuo, Dr. Michitoshi Hayashi, and Dr. Kaito Takahashi for serving as committee members for my MS.c thesis defense and for all the courses that I have taken to gain some basic knowledge that presented in this thesis.

This thesis has been completed under the instruction and guidance directly from my co-advisors, Dr. Jer-Lai Kuo and Dr. Qian-Rui Huang. With all of my respect and gratitude, I sincerely thank Dr. Kuo and Dr. Huang, for the patient guidance, encouragement and advices for my research over the past three years.

I would like to thank all of my friends in Taiwan for taking care of a foreign friend who got into so many troubles. I would also like to thank my other Vietnamese friends for always encouraging me remotely. Without all of your warm and kindly support, I could not make it this far to complete this thesis.

Last but not least, my biggest thank sends to my family for their unconditional love and support in everything that I do.

doi:10.6342/NTU202201978

doi:10.6342/NTU202201978

摘要

振動座標選擇能夠大幅影響非簡諧振動分析的收斂情形。理想情況下，我們會希望選擇的振動座標能夠對應到潛在的物理特徵，因而加速計算模擬的進行。在這個研究中，我們探討了在非簡諧振動分析中，幾種不同最佳化座標的方法。

在簡諧振動分析之中，簡正振動模式 (Normal mode) 是最常見且自然的選擇；然而若我們考慮非簡諧的位能面，各個簡正振動模式之間具有很強的耦合，因而使得對應的非簡諧振動計算的收斂十分緩慢。針對這類問題，Head 提出了「部分黑塞振動分析」(Partial Hessian Vibrational Analysis, PHVA) 對一部分原子、或是特定官能機團進行簡諧振動分析，取得對應的振動座標。這個方法在非簡諧振動分析中，能夠比傳統的簡正振動模式具有更好的收斂性。然而，這個方法需要人去手動將分子系統劃分區域，而這在許多系統中可能很難有效達成。參考軌域的局域化的方法，另一種更自動的座標選擇是「局部模式座標」(Local Mode Coordinates)。局部模式座標往往只涉及特定片段中的少數幾個原子的運動；這不僅符合人的直覺，同時使的我們能將對官能基的描述延伸到更大的系統中。然而，過度局域化會使結果嚴重偏離簡諧振動分析，因而使座標遠離其物理特徵。這意味著，最好的座標選擇，很可能介於簡正振動模式與完全局域化的局部模式之間。基於這個想法，1982 年 Thompson 和 Truhlar 嘗試通過最小化基態能量來獲得最佳化的振動座標；除此之外，Yagi 提出了一種泛用且穩定的最佳化演算法。

doi:10.6342/NTU202201978

在這份研究中，我們以有限基底表徵 (Finite Basis Representation, FBR) 描述振動波函數，基於雅可比掃描 (Jacobi Sweep) 與牛頓法進行最佳化的程序，透過變分原理來選擇使基態能量最小的座標。我們透過振動構型相互作用（VCI）和離散變量表示（DVR）的計算，對幾個氫鍵團塊進行了測試，以衡量該座標選擇的優勢。

關鍵字： optimized coordinates、localized coordinates、anharmonic vibration、IR spectra

doi:10.6342/NTU202201978

Abstract

The performance of reduced dimensional anharmonic vibrational calculations depends on the choice of vibrational coordinates. Ideally, the coordinates should be chosen to capture the underlying physics, interpret the vibrational features, and facilitate the computational simulations. In this study, we investigated different ideas on optimizing coordinates for anharmonic vibrational analysis. Normal mode coordinates are the most common choice for vibrational problems, however, for an anharmonic potential, the normal mode coordinates possess strong coupling constants among the modes and give slow convergence in n-mode potential representation and anharmonic calculations. One method of localizing the modes in specific functional groups is Partial Hessian vibrational analysis (PHVA), proposed by Head, which showed faster convergence compared with normal mode coordinates. However, this method is based on one' s chemical intuition, and it may be straightforward only for particular systems. Another more automatic approach which borrows ideas from

doi:10.6342/NTU202201978

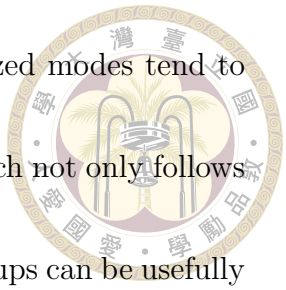

orbital localization techniques is local mode coordinates. Localized modes tend to involve only a few atom movements in identifiable fragments, which not only follows our intuition but also means that the description of functional groups can be usefully transferable to understand bigger systems. Though, over-localization could deviate substantially from the harmonic picture and produce an unphysical representation. It implies that the optimal coordinates should be somewhere between fully localized and fully delocalized coordinates. The idea of optimizing coordinates by minimizing ground state energy dates back to early work from Thompson and Truhlar in 1982; furthermore, a robust and general optimization algorithm was proposed by Yagi. Our approach used the wavefunction as the product of one-dimensional solutions in the finite basis representation (FBR). The variational principle was applied to choose the coordinates that minimize the ground state energy. The procedure to optimize was based on a combination of the Jacobi sweep and Newton method. Several hydrogen-bonded clusters were tested to benchmark the advantages of this scheme in the vibrational configuration interaction (VCI) and discrete variable representation (DVR) calculations.

Keywords: optimized coordinates, localized coordinates, anharmonic vibration, IR spectra

doi:10.6342/NTU202201978

Contents

doi:10.6342/NTU202201978

doi:10.6342/NTU202201978

doi:10.6342/NTU202201978

doi:10.6342/NTU202201978

List of Figures

doi:10.6342/NTU202201978

doi:10.6342/NTU202201978

doi:10.6342/NTU202201978

doi:10.6342/NTU202201978

List of Tables

doi:10.6342/NTU202201978

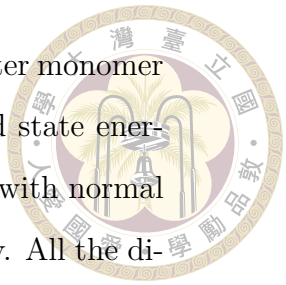

doi:10.6342/NTU202201978

doi:10.6342/NTU202201978

doi:10.6342/NTU202201978

Chapter 1 Introduction

Molecular spectra provide an abundance of information about the molecular structures, including the forces between the vibrating atoms, their electronic states, and electron distribution.[1] Vibrations are the fundamental motions of atomic nuclei in molecules, thus vibrational spectroscopy is one of the most powerful techniques to investigate molecular structures in solid, liquid, and gaseous forms. Assigning the spectra, however, is challenging due to the complexity of the inter-mode coupling of the vibrational motions. Therefore, vibrational simulations are widely used to analyze the vibrational features obtained from infrared (IR) spectroscopy experiments. To accurately model the vibrational spectra, several methods have been developed to go beyond the harmonic approximation. When the size of the molecules increases, full calculations of such large systems are computationally expensive due to the complexity of many-mode interactions. On the other hand, the experimental IR spectra frequently show the characteristics of a specific fragment or a functional group, indicating that sometimes, only a subset of localizing modes on specific fragment/ functional group is needed to interpret the spectral features.

The performance of reduced dimensional anharmonic vibrational calculations depends on the choice of vibrational coordinates. Ideally, the coordinates should be chosen to capture the underlying physics, interpret the vibrational features, and

doi:10.6342/NTU202201978

facilitate the computational simulations.

Normal mode coordinates are the most common choice for vibrational problems because they are mathematically convenient and provide a good zero-order picture when the potential is harmonic or nearly harmonic. However, for an anharmonic potential, the normal mode coordinates possess strong coupling constants among the modes and give slow convergence in n-mode potential representation and anharmonic calculations. [2] In addition, for the molecules with larger sizes, the normal mode coordinates are often delocalized, which means that it involves the motions of many nuclei in one normal mode. We believe that the couplings of modes are caused by the covalent bonds, therefore, it is hard to imagine those atoms which are far from each other should always move together as they are not connected by covalent bonds. In other words, normal mode coordinates are difficult to visualize and unfamiliar to our chemical intuition.

One method to localize the modes in specific functional groups is Partial Hessian vibrational analysis (PHVA), proposed by Head, [3] namely local normal mode coordinates. We have been using these local normal mode coordinates to investigate the vibrational spectroscopic signatures of many hydrogen-bonded clusters.[4, 5, 6, 7, 8, 9, 10] The results show that local normal mode coordinates converge faster than normal mode coordinates in the anharmonic calculations, and provide a more clear picture of the vibrational modes. Although in this approach, the difficulty is how to choose the fragments. Empirically, it is based on one's chemical intuition, and it may only be straightforward in particular systems. For example, it is counter-intuitive for some aromatic molecules to be divided into different fragments. Therefore, a more automatic way to define the localized coordinates should be developed.

doi:10.6342/NTU202201978

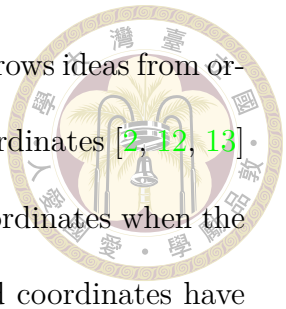

Another approach, namely local mode coordinates, which borrows ideas from orbital localization techniques. [11] Many works using localized coordinates [2, 12, 13] have proved that they have advantages over the normal mode coordinates when the potential is anharmonic. These studies showed that the localized coordinates have better convergence in n-mode expansion and in VCI calculations. Localized modes tend to involve only a few atom movements in identifiable fragments, which not only follows our intuition but also means that the description of local chemical units can be transferable in understanding bigger systems. However, over-localization could deviate substantially from the harmonic picture and produce unphysical representations. [14, 12, 2] It implies that the optimal coordinates should be somewhere between fully localized and fully delocalized coordinates.

This study aims to obtain the optimized set of coordinates by minimizing the ground state energy, the main idea of which dates back to Thompson and Truhlar [15] which was followed by the optimization algorithm proposed by Yagi.[16] Our approach used the wavefunction as the product of one-dimensional solutions in the finite basis representation (FBR) with the anharmonic potential included up to cubic and a part of quartic terms. The variational principle was applied to choose the coordinates that minimize the ground state energy. The procedure to optimize was based on a combination of the Jacobi sweep and the Newton method. After optimized coordinates are obtained, high-quality potential energy surface can be obtained by the discrete variable representation (DVR) method, which is very accurate but unfortunately computationally very expensive, therefore it should only be performed with low or reduced-dimensional anharmonic vibrational calculations and with a good set of coordinates. Several hydrogen-bonded clusters were tested

doi:10.6342/NTU202201978

to benchmark the advantages of localized and optimized coordinates in the vibrational configuration interaction (VCI) and discrete variable representation (DVR) calculations.

doi:10.6342/NTU202201978

Chapter 2 Theory

2.1 Quantum-Mechanical description of free molecules

Consider a molecule consisting of K nuclei (with masses M_k and charges $Z_k e$) and N electrons (mass m_e and charge $-e$). One can solve the time independent Schrödinger equation to describe the stationary states of the molecule:

$$\hat{H}\Psi = E\Psi \tag{2.1}$$

where the Hamiltonian is the sum of kinetic energy operator, denoted as $\hat{T}$, and potential energy operator, denoted as: $\hat{V}$,

$$\begin{aligned} \hat{H} &= \hat{T}_n + \hat{T}_e + \hat{V}(\mathbf{r}, \mathbf{R}) \\ &= \frac{-\hbar^2}{2} \sum_{k=1}^{K} \frac{1}{M_k} \nabla_k^2 - \frac{\hbar^2}{2m_e} \sum_{i=1}^{N} \nabla_i^2 + \hat{V}(\mathbf{r}, \mathbf{R}) \end{aligned} \tag{2.2}$$

in which, potential energy operator is described as:

$$\hat{V}(\mathbf{r}, \mathbf{R}) = \hat{V}_{n,n} + \hat{V}_{n,e} + \hat{V}_{e,e} \tag{2.3}$$

$(\mathbf{r}, \mathbf{R})$ are the coordinates of electrons and nuclei respectively.

doi:10.6342/NTU202201978

For convenience, atomic units are commonly used in quantum chemistry calculations. In atomic units, $m_e = \hbar = e = 1$. Substitute Hamiltonian operator into Schrödinger equation, we have

$$\left(\frac{-1}{2} \sum_{k=1}^{K} \frac{1}{M_k} \nabla_k^2 - \frac{1}{2} \sum_{i=1}^{N} \nabla_i^2 + \hat{V}(\mathbf{r}, \mathbf{R}) \right) \Psi(\mathbf{r}, \mathbf{R}) = E\Psi(\mathbf{r}, \mathbf{R}). \tag{2.4}$$

Note that the reference coordinates is chosen as laboratory frame.

2.2 Born-Oppenheimer approximation

The Schrödinger equation cannot be solved exactly even for the simplest molecule H_2^+. We need to introduce some approximations to simplify the equations. Born-Oppenheimer approximation is one of the most fundamental approximations in quantum mechanics calculations. The idea is that because of the mass difference (e.g. a proton is more than 1800 times as heavy as an electron), the nuclear motion is much slower than electronic motion. Based on this condition, in 1927 Max Born and J. Robert Oppenheimer proposed that the wavefunctions of atomic nuclei and electrons in a molecule can be treated separately. For the detailed derivation, please check this reference [1].

Under Born-Oppenheimer apprroximation, we have:

$$\Psi_{n,i}(\mathbf{r}, \mathbf{R}) = \phi_n^e(\mathbf{r}, \mathbf{R}) \times \chi_{n,i}(\mathbf{R}). \tag{2.5}$$

The Schrödinger equation is rewritten as two decoupled (electronic and nuclear)

doi:10.6342/NTU202201978

equations:

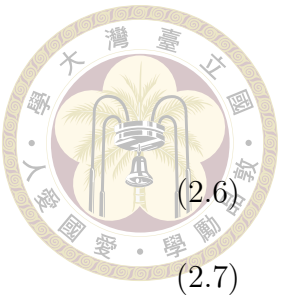

$$\hat{H}_0\phi_n^e(\mathbf{r}) = E_n^{(0)}\phi_n^e(\mathbf{r}) \text{ with } \hat{H}_0 = \hat{T}_e + \hat{V}(\mathbf{r},\mathbf{R}) \tag{2.6}$$

$$\left[\hat{T}_n + E_n^{(0)}(\mathbf{R})\right]\chi_{n,i}(\mathbf{R}) = E_{n,i}\chi_{n,i}(\mathbf{R}). \tag{2.7}$$

2.3 Nuclear motion

In the previous section, we have separated the electronic and nuclear wavefunctions. From now on, I will only discuss the nuclear motion. I will first consider the classical Hamiltonian to demonstrate that the translational and rotational motions can be separated from vibrational problems with some coordinate transformations for the classical kinetic energy expression. The Hamiltonian, then, will be converted to quantum mechanical Hamiltonian.

For polyatomic molecules, it is easier to describe using molecule-fixed reference frame, that is the molecule's center of mass and axes are fixed at equilibrium nuclear frame. The coordinates of i^{th} nuclei in molecule-fixed system are denoted by $\mathbf{r}_i = \{x_i, y_i, z_i\}$, where the center of mass of the molecule is chosen as $\mathbf{r}_{c.m} = \{0, 0, 0\}$. The coordinates of i^{th} nuclei in laboratory frame are denoted by $\mathbf{R}_i = \{X_i, Y_i, Z_i\}$ and $\mathbf{R}_{c.m} = \{X_{c.m}, Y_{c.m}, Z_{c.m}\}$. To transform from laboratory frame to molecule-fixed frame, we have:

$$\mathbf{R}_i = \mathbf{R}_{c.m} + \mathbf{r}_i. \tag{2.8}$$

Kinetic energy expression in molecule-fixed frame is:

$$T = \frac{1}{2}\left(\sum_{i=1}^{N} M_i V_i^2\right) = \frac{1}{2}\left(\sum_{i=1}^{N} M_i \dot{\mathbf{R}}_i^{\,2}\right). \tag{2.9}$$

doi:10.6342/NTU202201978

The molecule-fixed system rotates with an angular velocity ω around its center of mass, so we have to take it into account $d\mathbf{R}_i/dt$:

$$\dot{\mathbf{R}}_i = \dot{\mathbf{R}}_{c.m} + \dot{\mathbf{r}}_i + (\omega \times \mathbf{r}_i)\,. \tag{2.10}$$

Substitute into Eq. (2.9), then simplify we have:

$$T = \frac{1}{2} M \dot{\mathbf{R}}_{c.m}^2 + \frac{1}{2} \sum_i M_i \left(\omega \times \mathbf{r}_i\right)^2 + \frac{1}{2} \sum_i M_i v_i^2 + \omega . \sum_i M_i \left(\Delta \mathbf{r}_i \times \mathbf{v}_i\right) \tag{2.11}$$

in which:

- The first term describes the translations of molecule's center of mass.
- The second term describes the rotational energy of the molecule.
- The third term describes the vibrational energy of the molecule.
- The last term describes the Coriolis interaction between vibration and rotation.

This study only involves vibrations, therefore only the third term is included in the vibrational Hamiltonian with rigid rotor approximation to neglect the Coriolis coupling between vibration and rotation.

2.4 Vibrations of polyatomic molecules

Vibrational Hamiltonian for polyatomic molecules consist of N atoms is:

$$\hat{H} = \hat{T} + \hat{V} = \frac{-\hbar^2}{2} \sum_{i=1}^{3N} \frac{1}{m_i} \frac{\partial^2}{\partial x_i^2} + V(x_1, x_2, ..., x_{3N}). \tag{2.12}$$

where $V(x_1, x_2, ..., x_{3N})$ is $E_n^{(0)}(\mathbf{R})$ in the Eq. (2.7).

doi:10.6342/NTU202201978

The potential energy can be extended using Taylor expansion as:

$$\hat{V}(x_1, x_2, ..., x_{3N}) = V_0 + \sum_{i=1}^{3N} \left(\frac{\partial V}{\partial x_i}\right)_0 x_i + \frac{1}{2!} \sum_{ij}^{3N} \left(\frac{\partial^2 V}{\partial x_i \partial x_j}\right)_0 x_i x_j + \text{higher terms} \tag{2.13}$$

V_0 can be eliminated by choosing the zero of the energy at the equilibrium. At the equilibrium position, the energy must be a minimum, therefore all first derivatives vanish at this point $\left(\frac{\partial V}{\partial x_i}\right)_0 = f_i = 0$ with $i = 1, 2, ..., 3N$.

2.4.1 Harmonic approximation

For sufficiently small amplitudes of vibrations, the potential can be described quite well with the truncation at second derivatives, so that:

$$\hat{V} = \frac{1}{2} \sum_{ij}^{3N} f_{ij} x_i x_j \tag{2.14}$$

with $f_{ij} = \left(\frac{\partial^2 V}{\partial x_i x_j}\right)_0$ are constants. $V(x_i, ..., x_{3N})$ is a continuous function, therefore $f_{ij} = f_{ji}$.

Under harmonic approximation, the problem can be solved exactly. I will show the solutions in two cases, one dimensional and multi-dimensional vibration.

2.4.1.1 1D harmonic oscillator

Hamiltonian operator in 1D for harmonic oscillator is:

$$\hat{H} = \frac{\hat{p}^2}{2m} + \frac{m\omega^2 \hat{x}^2}{2} = \frac{1}{2m} \left(\frac{\hbar}{i} \frac{d}{dx}\right)^2 + \frac{m\omega^2 x^2}{2} \tag{2.15}$$

doi:10.6342/NTU202201978

where ω is the angular frequency of the classical oscillator related to the spring constant k in Hooke's law via $\omega = \sqrt{\frac{k}{m}}$.

The Schrödinger equation is given by:

$$\hat{H}\Psi(x) = E\Psi(x). \tag{2.16}$$

To solve the Schrödinger equation, it is convenient to introduce the so-called annihilation opertor ($\hat{a}$) and its adjoint operator, called the creation operator ($\hat{a}^\dagger$):

$$\hat{a} = \sqrt{\frac{m\omega}{2\hbar}}\left(x + \frac{ip}{m\omega}\right) \tag{2.17}$$

$$\hat{a}^\dagger = \sqrt{\frac{m\omega}{2\hbar}}\left(x - \frac{ip}{m\omega}\right). \tag{2.18}$$

The Hamiltonian operator can be rewritten as:

$$\hat{H} = \hbar\omega\left(\hat{a}^\dagger\hat{a} + \frac{1}{2}\right) = \hbar\omega\left(\hat{N} + \frac{1}{2}\right). \tag{2.19}$$

where $\hat{N} = \hat{a}^\dagger\hat{a}$ is number operator.

The energy eigenvalues are given by:

$$E_n = \left(n + \frac{1}{2}\right)\hbar\omega \text{ with } n = 0, 1, 2, ... \tag{2.20}$$

The energy of a harmonic oscillator is quantized into discrete values. Because the smallest possible value of n is zero, the ground state of the harmonic oscillator has:

$$E_0 = \frac{1}{2}\hbar\omega. \tag{2.21}$$

doi:10.6342/NTU202201978

The wavefunction for the eigenstate of harmonic oscillator is written as:

$$\Psi_n(x) = \frac{1}{\sqrt{2^n n! \sqrt{\sqrt{\pi} x_0}}} e^{-x^2/2x_0^2} H_n\left(\frac{x}{x_0}\right) \tag{2.22}$$

where $x_0 = \sqrt{\frac{\hbar}{m\omega}}$ and $H_n(x) = (-1)^n e^{x^2} \frac{d^n}{dx^n} e^{-x^2}$ is the Hermite polynomial.

2.4.1.2 Multi-dimensional harmonic oscillator

Under harmonic approximation, the Hamiltonian is written as:

$$\hat{H} = \frac{-\hbar^2}{2} \sum_{i=1}^{3N} \frac{1}{m_i} \frac{\partial^2}{\partial x_i^2} + \frac{1}{2} \sum_{ij}^{3N} f_{ij} x_i x_j, \tag{2.23}$$

in which, f_{ij} is the force constant matrix, or the so-called Hessian matrix, which is the second order derivative of the potential at the minimum.

One can write down the Newton's equation of motion along the direction of x_i:

$$x_i'' = \frac{F_i}{m_i} = -\sum_j \frac{f_{ij}}{m_i} x_j. \tag{2.24}$$

We can write $\frac{f_{ij}}{m_i}$ into a Matrix, and the differential equations become a matrix equation. However, we can see that $\frac{f_{ij}}{m_i}$ is not a symmetric matrix. To simplify the problem, we introduce the mass-weighted Cartesian coordinates $y_i = \sqrt{m_i} x_i$. The equation of motion is rewritten as:

$$y_i'' = -\sum_j \frac{f_{ij}}{\sqrt{m_i}\sqrt{m_j}} y_j = -\sum_j F_{ij} y_j. \tag{2.25}$$

Now, $F_{ij} = F_{ji}$, hence F is a symmetric matrix, whose eigenvalues are all real, and the eigenvectors form a unitary matrix. The diagonalization of F leads to the

doi:10.6342/NTU202201978

eigenvalues D and the unitary matrix P. Thus, we can define a new vector $\vec{z} = P^\dagger \vec{y}$, and rewrite the differential equations in $\vec{z}$:

$$\vec{z}'' = P^\dagger \vec{y}'' = -P^\dagger P D P^\dagger \vec{y} = -D\vec{z}. \tag{2.26}$$

Since D is a diagonal matrix, we can write it as:

$$D = \begin{bmatrix} \omega_1^2 & 0 & \cdots & 0 \\ 0 & \omega_2^2 & \cdots & 0 \\ \vdots & \vdots & \ddots & \vdots \\ 0 & 0 & \cdots & \omega_{3N}^2 \end{bmatrix} \tag{2.27}$$

Hence, we get $3N$ independent differential equations $z_i'' = -\omega_i^2 z_i$, which can be viewed as $3N$ indenpendent 1D Harmonic oscillators. The osillating frequencies should be ω_i. The unitary matrix P maps the mass-weighted cartesian coordinate y into a completely-independent coordinate z. We then call z as normal mode coordinates, and the eigenvectors Q in the unitary matrix P are called as normal modes.

From the vibrational energy of normal modes, the Hamiltonian can be written as:

$$\hat{H} = \frac{-\hbar^2}{2} \sum_{i=1}^{M} \frac{\partial^2}{\partial Q_i^2} + \frac{1}{2} \sum_{i=1}^{M} \omega_i^2 Q_i^2 \tag{2.28}$$

in which, $M = 3N - 6$ (or $M = 3N - 5$ for linear molecules) is the number of vibrations after separating vibrational motions from translational and rotational motions.

Due to the decoupling mediated by the normal modes, the Schrödinger equation

doi:10.6342/NTU202201978

$\hat{H}\Psi = E\Psi$ can be separated, using the product wavefunction:

$$\Psi_\nu(Q) = \prod_{\nu_i=1}^{M} \Psi_{\nu_i}(Q_i) \tag{2.29}$$

into M decoupled equations:

$$\frac{-\hbar^2}{2}\frac{\partial^2 \Psi_{\nu_i}(Q_i)}{\partial Q_i^2} + \frac{1}{2}\omega_i^2 Q_i^2 \Psi_{\nu_i}(Q_i) = E_i \Psi_{\nu_i}(Q_i). \tag{2.30}$$

The total vibrational energy is then:

$$E_v = \sum_{i=1}^{M} E_i \tag{2.31}$$

where E_i are the eigenvalues of the harmonic oscillator:

$$E_i = \hbar\omega_i \left(\nu_i + \frac{1}{2}\right) \text{ with } \nu_i = 0, 1, 2, ... \tag{2.32}$$

The eigenfunctions $\Psi_{\nu_i}(Q_i)$ using Hermite polynomial expression are:

$$\Psi_{\nu_i}(Q_i) = N_{\nu_i} H_{\nu_i}(\zeta_i) e^{-\zeta_i^2/2}, \tag{2.33}$$

where N_{ν_i} is a normalization factor, H_{ν_i} are the Hermite polynomials, and $\zeta_i = Q_i\sqrt{\omega_i/\hbar}$.

2.4.2 Anharmonic potential

For larger vibrational amplitudes, i.e., when vibrational quantum number n is bigger, the observed vibrational frequenicies ω_{vib} differ significantly from the constant ω_0 of the harmonic oscillator. It is because the molecular energy does not

doi:10.6342/NTU202201978

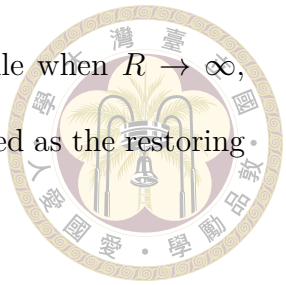

approach ∞ but converges to dissociation energy of the molecule when $R \to \infty$, resulting in the anharmonicity of the vibartions, which is described as the restoring force is no longer proportional to the displacement.

The model can be improved by including anharmonic terms in the potential. All of the higher terms in the potential energy surface beyond harmonic approximation contribute to the anharmonicity of the vibrations.

Potential energy operator in normal mode coordinates can be extended using Taylor series as:

$$\hat{V} = \frac{1}{2!}\sum_{i} f_{ii}\hat{Q}_i^{\,2} + \frac{1}{3!}\sum_{i,j,k} f_{ijk}\hat{Q}_i\hat{Q}_j\hat{Q}_k + \frac{1}{4!}\sum_{i,j,k,l} f_{i,j,k,l}\hat{Q}_i\hat{Q}_j\hat{Q}_k\hat{Q}_l + ... \tag{2.34}$$

where the coefficients are derivatives of the potential, shown as:

$$f_{ii} = \frac{\partial^2 V}{\partial Q_i^2},\ f_{ijk} = \frac{\partial^3 V}{\partial Q_i \partial Q_j \partial Q_k},\ f_{ijkl} = \frac{\partial^4 V}{\partial Q_i \partial Q_j \partial Q_k \partial Q_l}.$$

With an anharmonic potential, the Schrödinger equation can only be solved numerically.

2.4.2.1 1D anharmonic potential

Consider a diatomic molecule with only one vibrational mode, quartic potential is represented as:

$$\hat{V}(Q) = \frac{1}{2}f_{ii}\hat{Q}^2 + \frac{1}{6}f_{iii}\hat{Q}^3 + \frac{1}{24}f_{iiii}\hat{Q}^4. \tag{2.35}$$

The solution for the eigenvalues problem obtain from the first-order perturba-

doi:10.6342/NTU202201978

tion theory [1] is:

$$E_n = \hbar\omega\left(n+\frac{1}{2}\right) + \frac{3}{24}\frac{1}{2\beta^2}f_{iiii}\left[\left(n+\frac{1}{2}\right)^2+\frac{1}{4}\right]. \tag{2.36}$$

Within the first-order perturbation theory calculations, the first anharmonic term that contributes to the energy correction is quartic. Therefore, when considering an anharmonic effect, the potential should be included at least up to fourth-order.

Compare to the energy eigenvalues obtain from harmonic approximation, there are some impacts that anharmonic effect adds on to the vibrational spectra:

1. The energy levels are no longer equally spaced. Usually, they decrease for increasing quantum number n.

2. The transitions with $\Delta n = \pm 2, \pm 3, ...$ (overtones) are weakly allowed, while under harmonic approximation they are forbidden, which will be discussed in the next section (2.6).

Because of (1), the scaling factor (usually < 1) [17] is commonly used in the harmonic calculations in order to shift the bands to the right positions as in the experimental spectra.

2.4.2.2 Multi-dimensional anharmonic potential

Quartic potential for a molecule is expressed as Eq. (2.34).

The wavefunctions ansatz are chosen as the linear combination of the harmonic eigenfunctions:

$$\Psi = \sum_i c_i \Psi_i. \tag{2.37}$$

doi:10.6342/NTU202201978

Using a perturbation calculation, the energy eigenvalues for non-degenerate state are:

$$E_i^{\text{anh}} = E_i^{(0)} + \langle i^{(0)}|H'|i^{(0)}\rangle + \sum_k \frac{H_{ik}^2}{E_i^{(0)} - E_k^{(0)}}, \tag{2.38}$$

where $E_i^{(0)}$ are the harmonic energies, and H_{ik} is the coupling constant between state i and k.

If two vibrational levels are very close in the energy ($E_i^{(0)} \simeq E_k^{(0)}$), which is called degenerate states, the denominator will be diminished, resulting in a very large energy correction. There are several additional bands in the vibrational spectra that only can be explained by the anharmonic effect. I will show examples of Fermi resonance and combination bands in the following section.

2.4.2.3 Fermi Resonance and combination bands

Fermi resonance is a common phenomenon in molecular vibrational spectra. It happens when two states are close in energies and have the same symmetries leading to two states repelling each other (shifting in energies), and the darker state gains more intensity, while the brighter band decreases in intensity (shifting in intensities). Fermi resonance usually occurs between stretching fundamental and bending overtone. When two fundamental modes are excited simultaneously, it is called combination bands.

Both phenomenon cannot be addressed with only simple scaling factors, we must include the anharmonicity in the potential so that the overtones can be allowed in the selection rules.

doi:10.6342/NTU202201978

2.5 Methods for solving anharmonic vibration

Because of its complexity, the vibrational problems with an anharmonic potential can only be solved numerically. In this section, I will briefly introduce some commonly used methods to solve the nuclear Schrödinger equations, which are very similar to the methods that have been developed in the electronic structure theories.

2.5.1 Vibrational perturbation theory

Perturbation theory is the method to find an approximate solution to a problem involving a small parameter (small perturbed term). The total Hamiltonian is written as the sum of unperturbed and perturbed terms:

$$\hat{H} = \hat{H}_0 + \hat{H}' \tag{2.39}$$

in which, $\hat{H}_0$ is the Hamiltonian under harmonic approximation, which can be solved exactly, and $\hat{H}'$ includes all the higher terms in the potential. Applying vibrational second-order perturbation theory (VPT2), we have the energy of the state i as:

$$E_i = E_i^{(0)} + \langle \Psi_i | \hat{H}' | \Psi_i \rangle + \sum_k \frac{| \langle \Psi_i | \hat{H}' | \Psi_k \rangle |^2}{E_i^{(0)} - E_k^{(0)}}. \tag{2.40}$$

The advantage of VPT2 is that it is fast and gives good results near the equilibrium, and is suitable for large molecular calculations with the ratio between the coupling value and the energy difference between two states is small, which mean the perturbed term only makes a small changes to the system. However, the convergence is not guaranteed, and it is not a variational method, so the ground state

doi:10.6342/NTU202201978

energy is not a lower bound of exact ground state energy. In case of degenerate or nearly degenerate, VPT2 gives a very large correction term, so it is not a good method to deal with Fermi resonance and combination bands.

2.5.2 Vibrational self-consistent field

Vibrational self-consistent field (VSCF) is a mean field approach to solve vibrational Schrödinger equations.

A VSCF wavefunction is a product of one-dimensional functions:

$$\Psi_{VSCF}^{(n)} = \prod_{i=1}^{M} \phi_i^{(n)}(Q_i). \tag{2.41}$$

The Schrödinger equation for one mode is:

$$\left(\frac{-\hbar^2}{2} \frac{\partial^2 \phi_i^{(n)}(Q_i)}{\partial Q_i^2} + \tilde{V}_i^{(n)}(Q_i) \right) \phi_i^{(n)}(Q_i) = \epsilon_i^{(n)} \phi_i^{(n)}(Q_i) \tag{2.42}$$

where $\tilde{V}_i^{(n)}(Q_i)$ is the effective potential for mode Q_i:

$$\tilde{V}_i^{(n)}(Q_i) = \langle \prod_{j \neq i}^{M} \phi_j^{(n)}(Q_j) | \, \hat{V}(Q) \, | \prod_{j \neq i}^{M} \phi_j^{(n)}(Q_j) \rangle \, . \tag{2.43}$$

The total energy is written as:

$$\begin{aligned} E_n^{VSCF} &= \langle \Psi_{VSCF}^{(n)} | \, \hat{H} \, | \Psi_{VSCF}^{(n)} \rangle \\ &= -\frac{\hbar^2}{2} \sum_{i=1}^{M} \langle \phi_i^{(n)}(Q_i) | \, \frac{\partial^2 \phi_i^{(n)}(Q_i)}{\partial Q_i^2} \, | \phi_i^{(n)}(Q_i) \rangle + \langle \Psi_{VSCF}^{(n)} | \, \hat{V} \, | \Psi_{VSCF}^{(n)} \rangle \, . \end{aligned} \tag{2.44}$$

Applying variational method, we have to minimize the ground state energy

doi:10.6342/NTU202201978

with the constraint that the modals are normalized $\langle\phi_i^{(n)}|\phi_i^{(n)}\rangle = 1$. To do the minimization problem with a constraint, we use Lagrange multiplier method to obtain the VSCF equation:

$$\left[-\frac{\hbar^2}{2}\frac{\partial^2\phi_i^{(n)}(Q_i)}{\partial Q_i^2} + \langle\prod_{j\neq i}^{M}\phi_j^{(n)}|\,\hat{V}\,|\prod_{j\neq i}^{M}\phi_j^{(n)}\rangle\right]\phi_i^{(n)}(Q_i) = \epsilon_i^{(n)}\phi_i^{(n)}(Q_i) \tag{2.45}$$

and solve it iteratively.

VSCF provides good approximation for the ground state energy and low-lying states because it its wavefunction is anharmonic. However, for higher excited state, VSCF is not good enough since it lacks of explicit inter-mode coupling between two or more modes, as they only have mean field inter-mode coupling. It is also very expensive in terms of computational cost.

2.5.3 Finite basis representation

In finite basis representation (FBR) method, the vibrational Hamiltonian is written as the sum of one-mode Hamiltonian $\hat{H}_i(Q_i)$ and the coupling of the modes $\Delta V(Q)$:

$$\hat{H}(Q) = \sum_{i=1}^{f}\hat{H}_i(Q_i) + \Delta V(Q) \tag{2.46}$$

in which:

$$\hat{H}_i(Q_i) = -\frac{1}{2}\frac{\partial^2}{\partial Q_i^2} + c_{ii}Q_i^2 + c_{iii}Q_i^3 + c_{iiii}Q_i^4 \tag{2.47}$$

$$\Delta V(Q) = \sum_{i,j,k}^{f} c_{ijk}Q_iQ_jQ_k + \sum_{i,j,k,l}^{f} c_{ijkl}Q_iQ_jQ_kQ_l \tag{2.48}$$

where f is the number of selected modes.

doi:10.6342/NTU202201978

FBR wavefunction is the Hartree product of one-dimensional wavefunctions, as:

$$\Psi_n(Q) = \prod_{i=1}^{f} \phi_{n_i}^{(i)}(Q_i), \tag{2.49}$$

where $\phi_{n_i}^{(i)}(Q_i)$ is the numerical solution for one-dimensional anharmonic potential. Therefore, FBR wavefunction is closer to the exact answer compared to the harmonic basis.

The ground state energy is obtained by diagonalizing Hamiltonian matrix. Using FBR, the ground state energy is calculated without an iterative process as in VSCF, saving computational time. On the other hand, FBR and VSCF wavefunctions are similar because they have the same Hilbert space.

2.5.4 Vibrational configuration interaction

The idea of vibrational configuration interaction (VCI) is to describe the wavefunctions as the linear combination of basis functions at different states.

VCI wavefunction is written as:

$$|\Psi_{VCI}\rangle = c^{(0)} |\Psi^{(0)}\rangle + \sum_i c_i^{(r)} |\Psi_i^{(r)}\rangle + \sum_{ij} c_{ij}^{(rs)} |\Psi_{ij}^{(rs)}\rangle + \sum_{ijk} c_{ijk}^{(rst)} |\Psi_{ijk}^{(rst)}\rangle + ... \tag{2.50}$$

where r, s, and t are the number of quanta excited at the i, j and k normal modes. By including the full set of excited states, the full VCI wavefunction is obtained. However, full VCI calculations scale up quickly even for small size molecules and cannot be finished within a finite time. Therefore, in the calculations, we have to set the values for the max quantum number of excitations (n), and the number of

doi:10.6342/NTU202201978

simultaneously excited modes (m).

$$r + s + t + ... \leq n. \tag{2.51}$$

The basis sets are expressed as

$$|\Psi^{(0)}\rangle = |\phi_1^{(0)}\phi_2^{(0)}...\phi_i^{(0)}...\phi_M^{(0)}\rangle \tag{2.52}$$

$$|\Psi_i^{(r)}\rangle = |\phi_1^{(0)}\phi_2^{(0)}...\phi_i^{(r)}...\phi_M^{(0)}\rangle \tag{2.53}$$

$$|\Psi_{ij}^{(rs)}\rangle = |\phi_1^{(0)}\phi_2^{(0)}...\phi_i^{(r)}...\phi_j^{(s)}...\phi_M^{(0)}\rangle \tag{2.54}$$

$$|\Psi_{ijk}^{(rst)}\rangle = |\phi_1^{(0)}\phi_2^{(0)}...\phi_i^{(r)}...\phi_j^{(s)}...\phi_k^{(t)}...\phi_M^{(0)}\rangle \tag{2.55}$$

where $\phi_i^{(r)}$ is the harmonic oscillator eigenfunction or FBR 1D eigenfunction for normal mode Q_i.

Applying the variational method, we have the CI eigenvalue equation with the CI matrix:

$$c_i^{(n)} = \begin{bmatrix} \langle\Psi^{(0)}|\hat{H}|\Psi^{(0)}\rangle & \langle\Psi^{(0)}|\hat{H}|\Psi_i^{(r)}\rangle & \cdots & \langle\Psi(0)|\hat{H}|\Psi_{ijk...m}^{(rst...n)}\rangle \\ \langle\Psi_i^{(r)}|\hat{H}|\Psi^{(0)}\rangle & \langle\Psi_i^{(r)}|\hat{H}|\Psi_i^{(r)}\rangle & \cdots & \langle\Psi_i^{(r)}|\hat{H}|\Psi_{ijk...m}^{(rst...n)}\rangle \\ \vdots & \vdots & \ddots & \vdots \\ \langle\Psi_{ijk...m}^{(rst...n)}|\hat{H}|\Psi(0)\rangle & \langle\Psi_{ijk...m}^{(rst...n)}|\hat{H}|\Psi_i^{(r)}\rangle & \cdots & \langle\Psi_{ijk...m}^{(rst...n)}|\hat{H}|\Psi_{ijk...m}^{(rst...n)}\rangle \end{bmatrix}. \tag{2.56}$$

The VCI wavefunction are better than VSCF wavefunction because it includes the correlation energy. Full VCI calculations are highly accurate but very time consuming.

doi:10.6342/NTU202201978

2.5.5 Discrete variable representation

Discrete variable representation (DVR) method is a numerical method to solve partial differential equations. In DVR approach, the potential is scanned along the selected modes, thus its operator is represented as a diagonal matrix on the grid points. The grid points are chosen as Gauss-Hermite quadratures.

The Hamiltonian in DVR is expressed as

$$\hat{H} = \hat{T} + \hat{V} = -\frac{\hbar^2}{2}\sum_{i=1}^{M}\frac{1}{m_i}\nabla_i^2 + \begin{bmatrix} V(Q_1) & 0 & 0 & \cdots \\ 0 & V(Q_2) & 0 & \cdots \\ 0 & 0 & V(Q_3) & \cdots \\ \vdots & \vdots & \vdots & \ddots \end{bmatrix}. \tag{2.57}$$

The eigenvalues are obtained by diagonalizing the Hamiltonian with the Lanczos algorithm for sparse matrix.

The expression of potential energy surface on Gaussian Hermite is highly accurate, because with only N grid points, the polynomial is exact up to $(2N-1)^{th}$ order. However, the cost is scaled up exponentially with the number of nuclei. For M dimensional calculation, the total number of grid points is N^M. For such a huge matrix, the diagonalization takes a long time.

To save the computational cost with accuracy, the potential is approximated by the n-mode representation scheme:

$$\hat{V}(Q_i, Q_j, Q_k, ..) = V^{(0)} + \sum_i \Delta V_i^{(1)}(Q_i) + \sum_{ij} \Delta V_{ij}^{(2)}(Q_i, Q_j) + \sum_{ijk} \Delta V_{ijk}^{(3)}(Q_i, Q_j, Q_k) + ... \tag{2.58}$$

doi:10.6342/NTU202201978

where $V^{(0)}$ is the electronic energy at equilibrium point and $\Delta V_i^{(n)}$ is the n-mode contribution for modes i to the change in electronic energy, which can be obtained by subtracting all the contributions from its components:

$$\Delta V_i^{(1)}(Q_i) = V_i^{(1)}(Q_i) - V^{(0)} \tag{2.59}$$

$$\Delta V_{ij}^{(2)}(Q_i, Q_j) = V_{ij}^{(2)}(Q_i, Q_j) - \sum_i \Delta V_i^{(1)}(Q_i) - V^{(0)} \tag{2.60}$$

$$\Delta V_{ijk}^{(3)}(Q_i, Q_j, Q_k) = V_{ijk}^{(3)}(Q_i, Q_j, Q_k) - \Delta V_{ij}^{(2)}(Q_i, Q_j) - \Delta V_i^{(1)}(Q_i) - V^{(0)} \tag{2.61}$$

where $V_i^{(1)}(Q_i)$ is the one-dimensional cut of PES for the i mode, and $V_{ij}^{(2)}(Q_i, Q_j)$ is the two-dimensional cut of PES for the i and j mode and so on. Further details can be found in the original paper by Bowman and coworkers.[18]

2.6 Infrared spectra selection rules

Transitions are observed between different vibrational states depend on a number of selection rules, which determine the probability of the transition.

For a spontaneous transition from a higher state $n^{'}$ to a lower state $n^{''}$, the frequency of the emission light is:

$$\nu_{n^{'}n^{''}} = \frac{W_{n^{'}} - W_{n^{''}}}{h} \tag{2.62}$$

where $W_{n^{'}}$ and $W_{n^{''}}$ are the energies of the states $n^{'}$ and $n^{''}$, with the probability:

$$A_{n^{'}n^{''}} = \frac{64\pi^4 \nu_{n^{'}n^{''}}^3}{3h^2} |\mu_{n^{'}n^{''}}|^2. \tag{2.63}$$

The probability of absorption from state $n^{''}$ to state $n^{'}$ equals to the probability

doi:10.6342/NTU202201978

of the stimulation emission from state $n^{'}$ to state $n^{''}$:

$$B_{n^{''}n^{'}} = B_{n^{'}n^{''}} = \frac{8\pi^3}{3h^2}|\mu_{n^{'}n^{''}}|^2 \tag{2.64}$$

in which, $\mu_{n^{'}n^{''}}$ is the electric dipole moment:

$$(\mu_X)_{n^{'}n^{''}} = \int \Psi^*_{n^{'}} \mu_X \Psi_{n^{''}} dr \tag{2.65}$$

$$|\mu_{n^{'}n^{''}}|^2 = |(\mu_X)_{n^{'}n^{''}}|^2 + |(\mu_Y)_{n^{'}n^{''}}|^2 + |(\mu_Z)_{n^{'}n^{''}}|^2. \tag{2.66}$$

The electric dipole moment can be expanded as a power series in the coordinates of the atoms:

$$\mu_X = \mu_X^0 + \sum_{i=1}^{M} \mu_X^{(i)} Q_i + \text{ higher terms.} \tag{2.67}$$

Assume that higher terms contribution is very small and is neglected. Consider pure vibrational transition between state $n^{''}$ and state $n^{'}$, under harmonic approximation, the integral becomes:

$$\int \Psi^*_{n^{'}} \mu_X \Psi_{n^{''}} dR = \mu_X^0 \int \Psi^*_{n^{'}} \Psi_{n^{''}} dR + \sum_{i=1}^{M} \mu_X^{(i)} \int \Psi^*_{n^{'}} Q_i \Psi_{n^{''}} dR. \tag{2.68}$$

The first term vanishes because of the orthonormality of the wavefunctions, unless $n^{''} = n^{'}$. The integral in the second term can be written more explicitly as:

$$\begin{aligned} \int \Psi^*_{n^{'}} Q_i \Psi_{n^{''}} dR = & \int \Psi^*_{n_1^{'}}(Q_1) \Psi_{n_1^{''}}(Q_1) dQ_1 \\ & \times \int \Psi^*_{n_2^{'}}(Q_2) \Psi_{n_2^{''}}(Q_2) dQ_2 ... \times \int \Psi^*_{n_i^{'}}(Q_i) Q_i \Psi_{n_i^{''}}(Q_i) dQ_i ... \end{aligned} \tag{2.69}$$

Because of the orthonormality of the wavefuntions, the integral will vanish unless $n_1^{'} = n_1^{''}$, $n_2^{'} = n_2^{''}$, etc., with the exception of $n_i^{'}$ and $n_i^{''}$.

doi:10.6342/NTU202201978

$\int \Psi^*_{n_i'}(Q_i) Q_i \Psi_{n_i''}(Q_i) dQ_i \neq 0$ only for $n_i' - n_i'' = \Delta n = \pm 1$.

For anharmonic oscillators, the transitions with $\Delta n = \pm 2, \pm 3, ...$ are allowed, but with much smaller contributions than those for $\Delta n = \pm 1$.

doi:10.6342/NTU202201978

doi:10.6342/NTU202201978

Chapter 3 Vibrational Coordinates in Anharmonic Vibrational Analysis

From the previous chapter, we know how to calculate the normal mode coordinates. They are mathematically convenient choice, however, they give a slow convergence in anharmonic vibrational calculations. In this chapter, other possible choices of vibrational coordinates will be presented.

3.1 Local normal mode coordinates

One method to localize the modes in specific functional groups is Partial Hessian vibrational analysis (PHVA) proposed by Head.[3] Assume that the coupling between different fragments is negligible, the mass-weighted Hessian matrix is then sorted and divided into blocks, each block corresponding to one fragment:

$$H = \left[\begin{array}{c|c} H_{AA} & H_{AB} \\ \hline H_{BA} & H_{BB} \end{array}\right]. \tag{3.1}$$

doi:10.6342/NTU202201978

We have to find a unitary transformation matrix U that diagonalizes the block matrices in the mass-weighted Hessian:

$$\tilde{H} = U^T H U = \left[\begin{array}{c|c} \Lambda_{AA} & \tilde{H}_{AB} \\ \hline \tilde{H}_{BA} & \Lambda_{BB} \end{array}\right] \tag{3.2}$$

where Λ_{AA} and Λ_{BB} are diagonal eigenvalue matrices of H_{AA} and H_{BB} respectively; meanwhile, using U_{AA} and U_{BB}- the eigenvector of H_{AA} and H_{BB}, the unitary matrix U is therefore written as:

$$U = \begin{bmatrix} U_{AA} & 0 \\ 0 & U_{BB} \end{bmatrix}. \tag{3.3}$$

The column vectors in U are localized in either fragment A or fragment B, so we call them local normal mode coordinates; the frequencies of the vibrational local modes of each fragment should correspond to the square roots of eigenvalue in Λ_{AA} and Λ_{BB}.

We have been using this local normal mode coordinate to investigate the vibrational spectroscopic signatures of many hydrogen-bonded clusters. [4, 5, 6, 7, 8, 9, 10] The results show that local normal mode coordinates converge faster than normal mode coordinates in the anharmonic calculations, and provide clearer pictures of the vibrational modes. However, in this approach, the difficulty is on how to choose the fragments. Usually, it is based on one's chemical intuition, and it may be straightforward only for particular systems. For example, for some aromatic molecules, it is counter-intuitive to cut the ring into different fragments. Therefore, we should find a more automatic way to define the localized coordinates.

doi:10.6342/NTU202201978

3.2 Localized coordinates

Localized coordinates are unitary transformations of normal mode coordinates that maximize a localization criterion:

$$\tilde{Q}_i = \sum_{s=1}^{f} U_{si} Q_s, \tag{3.4}$$

where f is the number of selected modes.

Borrowing the orbital localization techniques, Jacob and Reiher proposed two ways to define the localization criteria $\zeta(\tilde{Q})$.[11]

1. The first way, which resembles the Pipek and Mezey localization,[19] is to maximize the sum of the squared of "atomic contributions" to the modes:

$$\zeta_{\text{at}}(\tilde{Q}) = \sum_{i=1}^{f} \sum_{p=1}^{N} \left(\sum_{\alpha=x,y,z} (\tilde{Q}_{i\alpha,p})^2 \right)^2 . \tag{3.5}$$

2. The second definition, which is similar to Boys localization, [20, 21, 22] is to maximize the distance between the "centers" of the modes:

$$\zeta_{\text{dist}} = \sum_{i=1}^{f} \left(\sum_{p=1}^{N} \sum_{\alpha=x,y,x} (\tilde{Q}_{i\alpha,p})^2 R_i \right)^2 \tag{3.6}$$

where R_i is the position vector of each nucleus with respect to the molecular origin.

The frequencies of localized modes are obtained from the diagonal terms of

doi:10.6342/NTU202201978

transformed Hessian matrix, which is:

$$\tilde{H} = \tilde{Q}^T H \tilde{Q}. \tag{3.7}$$

$\tilde{H}$ is no longer a diagonal matrix.

In their work, Jacob and Reiher also made a comparison between two different localization criteria and found that both approaches yield very similar localized modes. Therefore, in this thesis, I will only consider the atomic contribution criterion. The algorithm for maximizing the localization criterion using in this thesis is Jacobi sweep, which will be discussed in the next session.

Many works using localized coordinates [2, 12, 13] have proved it has advantages over the normal mode coordinates when the potential is anharmonic. Those works showed that the localized coordinates have better convergence in n-mode expansion and VCI calculations. Localized modes tend to involve only a few atoms' movements in identifiable fragments, which is not only followed our chemical intuition but also means that the description of local chemical units can be usefully transferable to understand the bigger systems. However, total localization does not benefit all vibrational modes. Over-localization could introduce a substantial harmonic coupling constant in the mass-weighted Hessian matrix. [14, 12, 2] It implies that the optimal coordinates should be somewhere between fully localized and fully delocalized coordinates.

doi:10.6342/NTU202201978

3.3 Optimized coordinates

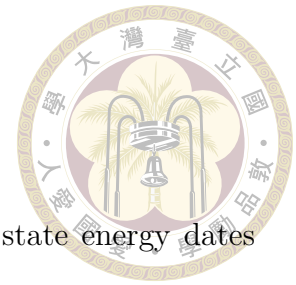

The idea of optimizing coordinates by minimizing ground state energy dates back to quite early work from Thompson and Truhlar in 1982, [15] and a robust and general optimization algorithm for VSCF energies is proposed by Yagi. [16]

Our approach is using the wavefunction as the product of one-dimensional solutions in finite basis representation (FBR).

3.3.1 Optimized coordinates

A new set of coordinates are defined as the unitary transformation of normal mode coordinates:

$$\tilde{Q}_i = \sum_{s=1}^{f} U_{si} Q_s, \tag{3.8}$$

with

$$U^\dagger U = U U^\dagger = \mathbf{1} \tag{3.9}$$

where $\mathbf{1}$ is a unit matrix. With the new set of coordinates, the Hamiltonian is rewritten as:

$$\hat{H}(\tilde{Q}) = \sum_{i=1}^{f} \hat{H}_i(\tilde{Q}_i) + \Delta V(\tilde{Q}) \tag{3.10}$$

where:

$$\hat{H}_i(\tilde{Q}_i) = -\frac{1}{2}\frac{\partial^2}{\partial \tilde{Q} i^2} + \tilde{c}_{ii}\tilde{Q}_i^2 + \tilde{c}_{iii}\tilde{Q}_i^3 \tag{3.11}$$

$$\Delta V(\tilde{Q}) = \sum_{i,j}^{f} \tilde{c}_{ij}\tilde{Q}_i\tilde{Q}_j + \sum_{i,j,k}^{f} \tilde{c}_{ijk}\tilde{Q}_i\tilde{Q}_j\tilde{Q}_k. \tag{3.12}$$

Under the unitary transformation, the approximate Hamiltonian is invariant.

doi:10.6342/NTU202201978

The FBR wavefunction in the new set of coordinates is:

$$\Psi_n(\tilde{Q}) = \prod_{i=1}^{f} \phi_{n_i}^{f}(\tilde{Q}_i). \tag{3.13}$$

The ground state energy in obtained by diagonalizing the Hamiltonian matrix. Apply the variational principle, the optimized coordinate is defined as the one to minimize the ground state energy.

3.3.2 Optimization algorithm

Our target is to apply the variational principle method to find the optimized coordinates, which are unitary transformations of normal mode coordinates that minimize the ground state energy. It is generally a difficult task, because there are $3N - 6$ vibrational modes making it becomes a many-variable optimization problem. In this session, I will give an overview of the algorithm to obtain optimized coordinates. The details will be discussed in the next few sub-sessions in this thesis.

The optimization algorithm suggested by Yagi and co-workers [16] is quite robust as it expresses the unitary transformation matrix as a product of Jacobi matrices, and does only one-dimensional optimization at a time. The one-variable minimization problem could be done in various ways. One efficient method is Newton's minimization with a good initial starting point obtained as the minimum value in Fourier series. The procedure is repeated for all coordinate pairs, thus we obtain the n one-dimensional solutions for the n-variable optimization problem. The whole process is then called Jacobi sweep. However, one Jacobi sweep is not guaranteed to provide the best answer for the optimization problem. Because the modes are

doi:10.6342/NTU202201978

coupled, the rotation of one pair affects all other coordinates. Therefore, we have to repeat the Jacobi sweep a few times to make sure that the energy is converged.

Given the overall idea, let's discuss the detailed implementation of the one-dimensional optimization process and the Jacobi sweep with the example of the water molecule to demonstrate the algorithm.

3.3.2.1 1D optimization

Now, we consider a two-mode system: there is only a single θ_{ij} value to determine, so the problem becomes one-dimensional optimization. Discrete cosine transform and Newton's minimization method are performed to obtain the optimal θ_{ij} for minimizing energy function in one dimension, denoted as $E_{1D}(\theta_{ij})$.

The rotational matrix for one pair coordinates (i, j) is written as:

$$U = \begin{bmatrix} \cos(\theta_{ij}) & -\sin(\theta_{ij}) \\ \sin(\theta_{ij}) & \cos(\theta_{ij}) \end{bmatrix}. \tag{3.14}$$

The new coordinates $(\tilde{Q}_i, \tilde{Q}_j)$ transformed from normal mode coordinates (Q_i, Q_j) are:

$$\tilde{Q}_i = Q_i \cos(\theta_{ij}) - Q_j \sin(\theta_{ij}) \tag{3.15}$$

$$\tilde{Q}_j = Q_i \sin(\theta_{ij}) + Q_j \cos(\theta_{ij}). \tag{3.16}$$

doi:10.6342/NTU202201978

The transformed force constants are:

$$\tilde{c}_{ij} = \sum_{s=1}^{f} U_{si} U_{sj} c_{ss} \tag{3.17}$$

$$\tilde{c}_{ijk} = \sum_{s,t,u=1}^{f} U_{si} U_{tj} U_{uk} c_{stu}. \tag{3.18}$$

With the new set of coordinates and force constants, the FBR 1D eigenvalue equation is rewritten and diagonalized to get the ground state energy. For each θ_{ij} value, we can find the corresponding ground state energy $E_{1D}(\theta_{ij})$.

The $E_{1D}(\theta_{ij})$ is scanned along θ_{ij} axis with evenly spaced grids, which are chosen as:

$$-\frac{\pi}{4} \leq \theta^{[n]} = \frac{n\pi}{2(2p+1)} \leq \frac{\pi}{4}, \text{ where } n = -p, -p+1, ..., p. \tag{3.19}$$

Since θ has its periodicity, the $E_{1D}(\theta_{ij})$ is the periodic function with the period of $\frac{\pi}{2}$. For n scanning grid points, we have n exact values of the ground state energies, and the function can be interpolated by fitting the discrete energies to a discrete cosine transform (DCT) with zero-padding in the inverse fast Fourier transform (FFT). The approximate discrete function by fitting is written as:

$$E_{1D}(\theta_{ij}) \approx \tilde{E}_{1D}(\theta_{ij}) = x_0 + \sum_{m=1}^{p} x_m \cos(\frac{\pi}{p+1} m\theta_{ij}) \tag{3.20}$$

where the expansion coefficient is:

$$x_m = \frac{1}{2p+1} \sum_{n=-p}^{p} E_{1D}(\theta_{ij}^{[n]}) \cos(\frac{\pi}{p+1} m\theta_{ij}^{[n]}). \tag{3.21}$$

By fitting, the number of data points increases, and it provides us a good guess for

doi:10.6342/NTU202201978

the minimum energy in one dimension, denoted as $\tilde{E}_{1D}^{\min}(\tilde{\theta}_{ij})$ at the $\tilde{\theta}_{ij}$ value.

To refine the result, Newton's minimization method is applied. Newton's method attempts to solve this problem by constructing a sequence θ_{ij}^k from the initial guess $\tilde{\theta}_{ij}$ that converges to a minimizer θ_{ij}^{1D} of the energy function $E_{1D}(\theta_{ij})$ by using a sequence of second-order Taylor expansion of $E_{1D}(\theta_{ij})$ around the iterates. The second-order Taylor expansion of $E_{1D}(\theta_{ij})$ around θ_{ij}^k is:

$$E_{1D}(\theta_{ij}^k + \Delta\theta_{ij}) = E_{1D}(\theta_{ij}^k) + E_{1D}^{'}(\theta_{ij}^k)\Delta\theta_{ij} + E_{1D}^{''}(\theta_{ij}^k)(\Delta\theta_{ij})^2. \tag{3.22}$$

To find the minimum of the function, the first derivation of the function over $\Delta\theta_{ij}$ must be 0:

$$\frac{d}{d\Delta\theta_{ij}}(E_{1D}(\theta_{ij}^k) + E_{1D}^{'}(\theta_{ij}^k)\Delta\theta_{ij} + E_{1D}^{''}(\theta_{ij}^k)(\Delta\theta_{ij})^2) = 0. \tag{3.23}$$

Therefore, the minimum is achieved for:

$$\Delta\theta_{ij} = -\frac{E_{1D}^{'}(\theta_{ij}^k)}{E_{1D}^{''}(\theta_{ij}^k)}. \tag{3.24}$$

We obtain the refine value for θ_{if} by performing Newton's iteration:

$$\theta_{ij}^{k+1} = \theta_{ij}^k - \frac{E_{1D}^{'}(\theta_{ij}^k)}{E_{1D}^{''}(\theta_{ij}^k)}, \tag{3.25}$$

in which, the derivatives are calculated by finite difference method:

$$E_{1D}^{'}(\theta_{ij}^k) = \frac{E_{1D}(\theta_{ij}^k + h) - E_{1D}(\theta_{ij}^k - h)}{2h} \tag{3.26}$$

$$E_{1D}^{''}(\theta_{ij}^k) = \frac{E_{1D}(\theta_{ij}^k - h) - 2E_{1D}(\theta_{ij}^k) + E_{1D}(\theta_{ij}^k + h)}{h^2}, \tag{3.27}$$

doi:10.6342/NTU202201978

where h is the step size in the finite difference method.

Take water molecule as an example:

There are three normal modes for a water monomer molecule, which are bending, symmetric stretching and asymmetric stretching modes. Consider the rotation of only two of the normal modes, while the third coordinate is fixed. In this example, the anharmonic potential included up to cubic terms only. The energy functions were scanned with seven grid points. Those grid points were then fitted to the discrete cosine transforms.

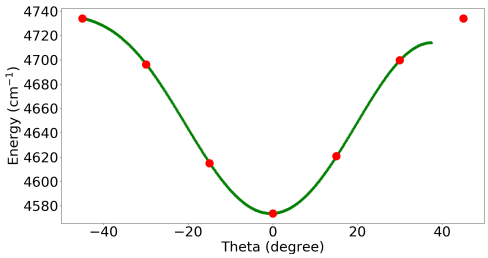

(a) $\tilde{E}_{1D}(\tilde{\theta}_{12})$

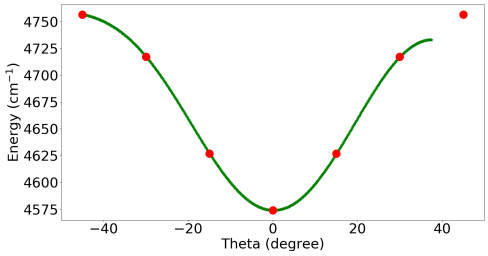

(b) $\tilde{E}_{1D}(\tilde{\theta}_{13})$

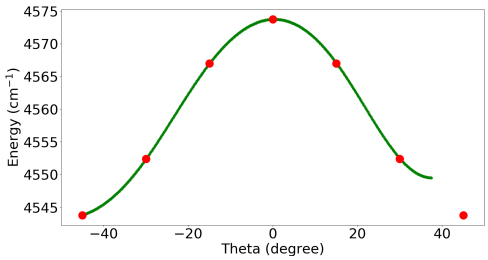

(c) $\tilde{E}_{1D}(\tilde{\theta}_{23})$

Figure 3.1: The energy is one-dimensional function of theta. The red points were the scanning points of the one-dimensional energy function and the green points were the fitting points to the discrete cosine transforms.

doi:10.6342/NTU202201978

As shown in the Figure 3.1 above, we know roughly the shape of one-dimensional potential and the minimum points could be located and shown in the table as the initial guess to do Newton's minimization method.

(i,j)	$\tilde{E}_{1D}(\tilde{\theta}_{ij})(\mathrm{cm}^{-1})$	$\tilde{\theta}_{ij}$(degree)
(1,2)	4573.6026	0.7714
(1,3)	4573.7158	0.0642
(2,3)	4543.7852	-45.0000

Table 3.1: Initial guess obtained from discrete cosine transform

From the initial guess in table 3.1, Newton's minimization method was performed to refine the result.

3.3.2.2 Jacobi Sweep

From the previous sub-section, we know how to obtain the optimal value for one coordinate pair. For a molecule with a set, or subset, of f modes, there are $F = \frac{f(f-1)}{2}$ coordinate pairs. To do the F variable optimization problem, Yagi proposed to solve it iteratively by doing only one-dimensional problem at a time and fixed the other pairs by doing Jacobi rotations.

The size of the Jacobi matrix for the rotation of coordinate pair (i, j) should be $f \times f$, with the matrix elements:

$$U_{ii} = U_{jj} = \cos(\theta_{ij}) \tag{3.28}$$

$$U_{ij} = -U_{ji} = \sin(\theta_{ij}) \tag{3.29}$$

and, otherwise,

$$U_{kl} = \delta_{kl}. \tag{3.30}$$

doi:10.6342/NTU202201978

The unitary transformation matrix for one sweep is constructed as the product of Jacobi matrices:

$$u = \prod_{i=1}^{F} U_i. \tag{3.31}$$

Thus, for M Jacobi sweeps, the unitary transformation matrix is:

$$U = \prod_{m=1}^{M} u^{(m)}. \tag{3.32}$$

Since the unitary matrices do not commute, the product is arranged in such a way that the smaller index m comes to the left. With the expression of U, one Jacobi sweep loops for all over the coordinate pairs and do one-dimensional minization at one time. The process is repeated a few times to make sure that the ground state energy is converged.

Continue the previous example of water molecule:

For one Jacobi sweep, the unitary transformation matrix was written as:

$$u = \begin{bmatrix} \cos(\theta_{12}) & -\sin(\theta_{12}) & 0 \\ \sin(\theta_{12}) & \cos(\theta_{12}) & 0 \\ 0 & 0 & 1 \end{bmatrix} \times \begin{bmatrix} \cos(\theta_{13}) & 0 & -\sin(\theta_{13}) \\ 0 & 1 & 0 \\ \sin(\theta_{13}) & 0 & \cos(\theta_{13}) \end{bmatrix} \times \begin{bmatrix} 1 & 0 & 0 \\ 0 & \cos(\theta_{23}) & -\sin(\theta_{23}) \\ 0 & \sin(\theta_{23}) & \cos(\theta_{23}) \end{bmatrix}. \tag{3.33}$$

For n Jacobi sweeps, the unitary transformation matrix was written as in Eq. (3.32).

Applied Jacobi sweeps on water molecules, we obtained:

sweep	E_{GS}	ΔE_{GS}	θ_{12}	θ_{13}	θ_{23}
0	4573.7156	0	0	0	0
1	4543.9017	29.8138	0.6936	-0.0002	-45.0143
2	4543.7881	0.1136	-0.4786	-0.0079	0.0023
3	4543.7881	0.0000	-0.0209	-0.0220	-0.0043

Table 3.2: Jacobi sweeps for water molecule. The energies are in cm^{-1}, and the theta are in degree.

doi:10.6342/NTU202201978

As seen on the table 3.2, the ground state energy converged after three Jacobi sweeps with the convergence $\leq 10^{-3}$ cm^{-1}.

One can also use the Jacobi sweep and Newton's method to obtain the localized coordinates with just one modified step: instead of maximizing localization criterion, we can minimize its negative function ($\zeta_{\text{at}}(\tilde{Q})$).

3.4 Other ideas

Besides, there are also other approaches to improve from the localized coordinates by limiting the harmonic coupling.[23, 24] Another idea, [25] from the same authors of localized metric with constrained optimization, [24] is to minimize the off-diagonal anharmonic coupling and maximize the diagonal anharmonicity of $M + 1$ Hessian, where M is the number of the selected modes. From the spirit of optimizing coordinates based on ground state energies, in 2004, Yagi and coworkers [26] proposed the idea of stage-average optimal coordinates by including the fundamental transition states of the targeted motions with an equal weight in the optimization procedure. There have been a several following works [27, 28, 29, 30] from the same group moving toward to the bigger size molecules.

doi:10.6342/NTU202201978

doi:10.6342/NTU202201978

Chapter 4 Computational Details

Quantum chemical calculations were performed using Gaussian16 [31] program to determine the electronic structures and normal mode coordinates. The geometric structures were optimized at the MP2/aug-cc-pvdz level. The harmonic frequencies were obtained by diagonalizing the mass-weighted Hessian matrix, which is the second-order derivative of the total energy.

In coordinate optimization process, the anharmonic potential was obtained by Taylor's expansion truncated at the forth order.The anharmonic vibrational Hamiltonian included all the cubic terms and part of the quartic terms, which were only up to three different modes, in the potential energy operator, where the third and fourth-order force constants were calculated using finite difference methods from the analytical second-order derivatives. The step size to do finite difference method was chosen as 0.01 Å.

The optimization algorithm was a combination of Jacobi's sweep and Newton's minimization method, and the whole many-variable optimization problem could be treated as many one-dimensional minimization problems. The one-dimensional energy function was scanned along θ direction with seven evenly spaced grid points. The function can be interpolated by fitting the seven scanning points to a discrete

doi:10.6342/NTU202201978

cosine transform to get one hundred times data points. The approximated theta value as the point corresponding to the lowest energy of the fitted function was chosen to be the initial guess of the Newton's minimization step. In Newton's method, the step size to do finite difference method was chosen as 0.0005 Å. The convergences were 10^{-6} and 10^{-3} cm^{-1} for the derivatives in Newton's method and the ground state energies in Jacobi's sweep, respectively.

In order to compared the results with the experiments, the vibrational spectra were simulated with DVR and VCI methods, which were implemented by Dr. Qian-Rui Huang, the detailed description can be found in the early work. [10, 32, 33] The anharmonic potential for VCI calculations were the same quartic potentials as reported above. The basis were chosen as six for the maximum number of excitations (n) and four for the number of simultaneously excited modes (m). In DVR method, the anharmonic potentials were scanned along the selected modes, which were five points for bending, seven points for stretching modes. In both methods, the matrices are very sparse and can be diagonalized using ARPACK[34] in the SciPy package to obtain the ground state and low-lying excited states with the eigenvalues up to 5000 cm^{-1}. The Fermi golden rule was applied to evaluate the absorption intensities of vibrational transitions.

doi:10.6342/NTU202201978

Chapter 5 Results and Discussion

In this chapter, our results are presented as follows: First, the differences between HO and FBR basis will be shown and discussed to understand our choice of the wavefunction in optimizing coordinates. After that, I will show the illustration of the optimization process and the performance of optimized coordinates and localized coordinates in VCI and DVR calculations with the example of water monomer and water dimer molecules. Then, four sets of coordinates, which are normal mode coordinates, local normal mode coordinates, localized coordinates and optimized coordinates will be examine in the study of Fermi resonance patterns in some hydrogen-bonded cluster, i.e. ammonia and methylamine clusters to demonstrate how the choice of coordinates can help to reduce the degree of freedom in VCI or DVR calculations with qualitative description of the main features of the spectra.

Since our study mainly focused on Fermi resonance, which is due to the coupling between the stretching fundamental and bending overtone, only those high-frequency motions were considered in our examples. Besides, the low-frequency modes are normally floppy, therefore they are believed to be better described with curvilinear coordinates than with rectilinear coordinates. The unitary transformation from

doi:10.6342/NTU202201978

normal mode coordinates cannot help to solve this problem. Thus, this study only focused on the high-frequency vibrational modes.

Each test system will be discussed in turn.

5.1 Differences between HO and FBR basis

The Hamiltonian can be written as the sum of one-dimensional Hamiltonian and the coupling of the modes, and wavefunction can be expressed as the product of one-dimensional harmonic oscillator (HO) wavefunctions or one-dimensional finite basis representation (FBR) wavefunctions. Under the harmonic approximation, both choices should give us the same results. However, the results will be different if the anharmonic effects are considered.

Table 5.1 shows the ground state energy in normal mode coordinates in different basis representation before and after diagonalizing the CI matrix, which includes only up to one-quanta basis kets for the purpose of optimizing coordinates. In Table 5.1, $\langle 0|\hat{H}|0\rangle$ is the zero-quanta basis ket and E_{GS} is the ground state energy calculated by diagonalizing the CI matrix in either HO or FBR representation. The difference between $\langle 0|\hat{H}|0\rangle$ and E_{GS} is caused by the coupling between the zero and one quanta basis kets that push the ground state energy lower. With harmonic potential (k_2 only), FBR and HO basis gave us the same results. Since there is no cross term in normal mode coordinates under harmonic approximation, the matrices are already in diagonal form, the ground state energies are simply half of the sum of the normal mode frequencies. When the cubic terms of the potential were included, HO and FBR gave us different results. In HO basis, the $\langle 0|\hat{H}|0\rangle$ value did not

doi:10.6342/NTU202201978

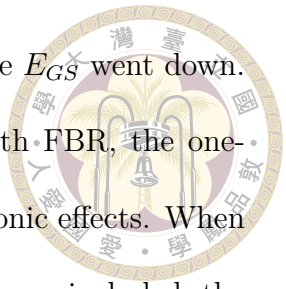

change compared to the value of harmonic potential, however, the E_{GS} went down. In FBR basis, both $\langle 0|\hat{H}|0\rangle$ and E_{GS} values decreased since with FBR, the one-dimensional wavefunctions already take into account the anharmonic effects. When the cubic terms of the potential were excluded and the quartic terms included, the energies increased, however, there was no change in the values before and after diagonalizing the matrix in both representations. Because the zero and one quanta basis kets couple through the odd operators, therefore, only the cubic terms have the contribution of the couplings between those basis kets. The last column shows the results of the quartic potentials which were actually used in our calculations. It is clearly seen that FBR gave lower ground state energy. Furthermore, in the FBR, the values before and after diagonalizing the CI matrix are closer, indicating that the couplings are smaller on FBR basis than on harmonic basis. Hence, FBR gave us a better zeroth-order picture and faster convergence than the harmonic basis did.

5.2 Optimization process and the performance of optimized coordinates and localized coordinates in VCI and DVR calculations

As one of the most studied clusters with an abundance of available data for comparison, the water clusters, i.e. water monomer and water dimer molecule, were our first test cases to illustrate the optimization process and its advantages in the performances of VCI and DVR calculations.

doi:10.6342/NTU202201978

5.2.1 Water monomer

The optimization procedure was repeated as in chapter 3.3.3 with an anharmonic potential including cubic and part of quartic terms up to three-mode different. The one-dimensional energy functions were scanned and fitted to discrete cosine transforms as shown in the Figure 5.1 and the results of Jacobi's sweep for water monomer molecule are shown in Table 5.2. The energy convergence criterion was reached within three Jacobi sweeps. Comparing cubic (see Figure 3.1) and quartic (see Figure 5.1) potentials, they shared the same shape of the potential, only differed in the magnitude of the energy. The ground-state energy decreased when modes 2 and 3, i.e. two stretching modes, were mixed. The similar results were obtained in Yagi's work [16]. The resulting coordinates were two degenerate stretching modes localized on the hydrogen bond and the bending mode remaining the same as normal mode coordinates. The visualization of the vibrational modes are shown in Figure A.1.

The new set of force constants in optimized coordinates were obtained using the unitary transformation matrix and compared to those in normal mode coordinates. Since only two stretching mode were rotated after the optimization process, the Table 5.3 only shows the force constants of those two modes in quartic potential. In normal mode coordinates, there was no cross-term in the second order force constants, while the rotational matrix introduced a harmonic coupling of -134 cm^{-1} in the optimized coordinates. However, some anharmonic coupling constants found in normal mode coordinates were minimized in the optimized coordinates and concentrated in the diagonal terms. The total coupling constants in normal mode

doi:10.6342/NTU202201978

coordinates was bigger than the total coupling constants in optimized coordinates, indicating the wavefunctions with the optimized coordinates are better.

The VCI calculations with truncated basis sets were performed and compared between two sets of coordinates. The results are presented in Table 5.4. In the full calculations, VCI[3]-(8) and oc-VCI[3]-(8), both sets of coordinates gave the same results. However, in the truncated-basis set calculations, the optimized coordinates converged faster than the normal mode coordinates did.

After determining the set of optimized coordinates, a better quality of the PES can be obtained by the DVR method. The (small size) Hamiltonian matrix before diagonalization are shown in Table 5.5. The water monomer molecules possess a C_{2v} symmetry, with the bending and symmetric stretching modes belong to A_1 representation and the asymmetric stretching mode belongs to B_2 representation. Due to the symmetry, in normal mode coordinates, the bending fundamental and overtone basis kets ($|1,0,0\rangle$ and $|2,0,0\rangle$) only couple with the symmetric stretching fundamental ($|0,1,0\rangle$). Therefore, in the DVR calculation with normal mode coordinates, there are some zero values in the off-diagonal matrix elements since there is no coupling between bending fundamental and overtone basis kets and asymmetric stretching basis ket ($|0,0,1\rangle$). However, in the optimized coordinates, two stretching modes are localized and degenerate, hence, the symmetry of those two modes are broken. The bending basis kets couples with both stretching fundamental basis kets with the same magnitude of the coupling constants. In normal mode coordinates, only the symmetric stretching fundamental basis ket couple strongly with the zero quanta basis ket, while in optimized coordinates, both stretching fundamental basis kets couple with the zero quanta basis ket with the same coupling constants at about

doi:10.6342/NTU202201978

20 cm^{-1}, and they are much smaller in magnitude than the coupling constant in the normal mode case, at -250 cm^{-1}. Some big coupling constants in the normal mode coordinates, i.e. between stretching fundamental and stretching overtone basis kets, for both symmetric and asymmetric stretching, also become smaller in the optimized coordinates.

After diagonalizing the Hamiltonian matrix to get the peak positions, the intensities were calculated using Fermi golden rule. The contribution of the basis kets to the eigenstates are computed by the inner product between the eigenstates and the basis kets. The results of peak positions, intensities and projection are shown in the Table 5.6. The notation $|n_i, n_j, n_k\rangle$ is the basis ket in DVR calculation; where n_i, n_j, n_k are the FBR 1D eigenfunctions, three number inside the ket are corresponding to the quantum number of bending and two stretching modes, respectively. From Table 5.6, for the simulated spectra using DVR method, both normal mode coordinates and optimized coordinates gave similar results of the peak positions and intensities. However, the contributions of the basis kets to the eigenstates in two sets of coordinates were different. In the optimized coordinates case, the two stretching fundamental basis kets were degenerate, therefore, their contributions to the eigenstates were similar.

5.2.2 Water dimer

Our second test case was the water dimer molecule. There are 12 vibrational motions for a water dimer molecule. The first six degrees of freedom are intermolecular motions with low frequencies. Therefore, in this test case, only the six high-frequency vibrational modes, which are two bending and four stretching modes,

doi:10.6342/NTU202201978

were included in the optimization process.

Adapting the idea of tuning localization frequency window, [35] the six degrees of freedom were divided into two sub-groups (two bending and four stretching modes), in order to reduce the number of theta variables in the optimization process and to prevent the mixing of bending and stretching modes leading to some unphysical local modes.

The optimizations with both cubic and quartic potentials were tested. Similar to the results of the water monomer molecule, the one-dimensional energy functions with both potentials had the same shape, only differed in the magnitudes of energies. The normal mode coordinates and optimized coordinates of the water dimer are shown in Figure A.4. In the normal mode coordinates, all the vibrational motions are delocalized. In the optimized coordinates, the bending frequencies did not change much compared with the bending frequencies in normal mode coordinates but they were localized on each monomer. All four stretching modes were localized on the hydrogen bonds, with two stretchings of the proton-acceptor were degenerate.

Table 5.7 presents the force constants of four stretching modes before and after rotating the coordinates.The cubic potential extended by Taylor series converged much faster in optimized coordinates than in normal mode coordinates. Although in optimized coordinates, some harmonic couplings arose from rotating the coordinates, the anharmonic couplings were much smaller than those anharmonic couplings in normal mode coordinates, suggesting that the set of optimized coordinates is a better choice.

In addition, the localized coordinates were also tested for the water dimer

doi:10.6342/NTU202201978

molecule. The results were comparable to the optimized coordinates, but maximizing the localization criterion does not require an anharmonic potential, therefore, the localization process was much faster than optimization process. The visualizations of the localized coordinates are shown in the Figure A.4.

5.3 Fermi resonance study assisted by the choices of coordinates

Fermi resonance is one of the quantum mechanical mechanisms, which leads to the complexity of the vibrational spectroscopic in the X-H (X = O, N, and C) stretching frequency region. [5, 36, 37, 38, 39] The difficulty in studying Fermi resonance is mainly due to:

- The sensitivity of the intensity borrowing depends on the position of stretching fundamental transition, which carries the main intensity of the bands. This problem can be improved by getting a better quality potential energy surface using DVR with a high-level of theory method.

- In normal mode coordinates, the coupling constants between stretching fundamental and bending like overtones are delocalized due to the delocalization of the vibrational modes among the whole molecule.

This thesis mainly focused on solving the second problem with the use of optimized and localized coordinates.

Motivated by our recent publications on understanding Fermi resonance in the complex vibrational spectra of amino and methyl groups in hydrogen-bonded sys-

doi:10.6342/NTU202201978

tems, [40, 6, 8, 7] ammonia and methylamine clusters were chosen as our tested cases to demonstrate the performance of four sets of coordinates: normal mode coordinates (NC), local normal mode coordinates (LNM), localized coordinates (LC), and optimized coordinates (OC) in studying Fermi resonance patterns. The results are presented in the next sub-sections of this chapter.

5.3.1 Ammonia cluster

5.3.1.1 Ammonia dimer

For ammonia dimer molecule, ten vibrational motions including four bending modes and six stretching modes were considered and divided into two sub-groups.

The normal mode coordinates (NC), local normal mode coordinates (LNM), localized coordinates (LC), and optimized coordinates (OC) for ammonia dimer molecule are shown in the Figure A.5, A.6, A.7 and A.8 respectively. In NC, all the vibrational motions were delocalized for the whole molecule. In LNM, the vibrational motions were localized on each monomer. The OC and LC gave quite similar results, in which, two bending modes were localized on the proton-donor monomer, other two were localized on the proton-acceptor monomer, and six stretching were localized on the six hydrogen bonds.

Table 5.8, 5.9, 5.10 presents the ten-dimensional VCI calculations with normal mode coordinates, optimized coordinates and localized coordinates for ammonia dimer molecule. In this case, it was shown that in the reduced-dimensional VCI calculations, at the size of basis set $[6]-(6)$, the optimized coordinates and localized coordinates gave similar results as the normal mode coordinates did. Slight

doi:10.6342/NTU202201978

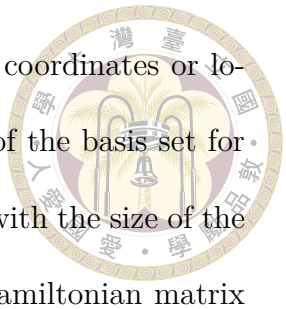

improvements of the MAD were obtained when using optimized coordinates or localized coordinates. Both sets of coordinates suggested the size of the basis set for VCI calculation at [3]-(5) with the convergence less than 3 cm^{-1} with the size of the Hamiltonian matrix were just 5% compared to the size of the Hamiltonian matrix with the basis set [6]-(6).

The simulated spectra of the ammonia dimer molecule by VCI methods with four different sets of coordinates are shown in the Figure 5.2. From Figure 5.2, the peak positions were consistent in all spectra simulated with different sets of coordinates using ten degrees of freedom. The intensity ratio of the two main peaks were flipped in OC and LC pictures compared to NC and LNM spectra.

As learned from previous work, [7] the spectra features are mainly contributed by proton-donor ammonia. Therefore, five-dimensional calculations on proton-donor and five-dimensional calculations on proton-acceptor in LNM, LC and OC were performed to investigate the contribution of proton-donor and proton-acceptor to the spectra and were compared with ten-dimensional calculation in NC. The results are presented in the Figure 5.3. The VCI calculation with only five vibrational modes on the proton-donor monomer using LNM, LC and OC captured the Fermi resonance patterns of ammonia dimer molecule. The small peaks at around 3350 cm^{-1} and 3490 cm^{-1} obtained in NC with ten modes are the stretching fundamental transitions in proton-acceptor. Therefore, we can conclude that the contributions of proton-acceptor ammonia on the spectra are very minor.

In order to have a qualitative comparison with the experimental result, the DVR reduced dimensional calculations were performed with four different sets of

doi:10.6342/NTU202201978

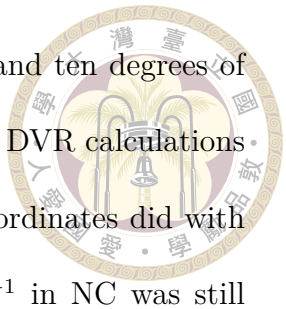

coordinates with five degrees of freedom for LNM, LC and OC and ten degrees of freedom for NC. The results are presented in the Figure 5.4. The DVR calculations with LNM, LC and OC gave similar spectra as normal mode coordinates did with a smaller degree of freedom. A small peak at about 3467 cm^{-1} in NC was still there in the LNM, LC, and OC spectra but with a very weak intensity because the transition dipole moment were cancelled out (see Table 5.11). Better agreement with the experimental result can be achieved by using higher levels of theory with bigger size basis sets. [7]

5.3.1.2 Ammonia trimer

For ammonia trimer molecule, the hydrogen bond is stronger than the ammonia dimer molecule, each monomer is both proton-donor and prton-acceptor. Fifteen vibrational motions including six bending and nine stretching modes were considered in the optimization and localization processes and they were divided into two sub-groups.

The visualization of vibrational motions in four sets of coordinates are shown in the Figure A.9, A.10, A.11 and A.12 corresponding to NC, LNM, LC and OC, respectively. Similar to the results obtained in ammonia dimer, all the vibrational motions were delocalized for the whole molecule in NC and were localized on each monomer in LNM. The stretching modes were localized on the hydrogen bonds with the frequencies were degenerated for six free NH modes and triply degenerated for three bonded NH modes, and two bending modes localized in each monomer with two sets of triply degenerated frequencies in both LC and OC.

doi:10.6342/NTU202201978

The VCI calculations with fifteen degrees of freedom in NC, LNM, LC and OC were performed. Besides, similar to the analysis had been done for ammonia dimer, the VCI calculations with five degrees of freedom on an ammonia monomer in LNM, LC and OC were also performed and compared to the higher dimensional calculations. The results are shown in the Figure 5.5. As we can see from the spectra in orange, the VCI calculation with fifteen modes in NC gave a very bad result, while the results of the VCI calculations with LNM, OC and LC were quite similar and more comparable with the experimental spectra. The spectra in blue, which are smaller calculations with only five modes on an ammonia monomer still captured the main features of the spectra calculated by fifteen modes but with weaker intensities. LNM, LC and OC gave the three sets of triply degenerate frequencies for each ammonia monomer, therefore, each monomer had the equally contribution to the spectra features obtained in fifteen dimensional calculations.

In addition, the DVR calculation with OC using five degrees of freedom was performed and compared with the VCI calculations with OC using five and fifteen modes and the experimental spectra as shown in the Figure 5.6. With a higher quality potential energy surface, the DVR calculation with optimized coordinates using five modes gave us a more comparable picture to the experimental result. [7]

5.3.2 Methylamine cluster

As found in the previous work, [40] the couplings between amino and methyl functional groups in methylamine cluster are negligible, therefore they can be treated separately in the vibrational spectrum problems.

doi:10.6342/NTU202201978

5.3.2.1 Methylamine dimer

For methylamine dimer molecule, six and twelve vibrational motions were considered for the amino and methyl groups, respectively. The visualization of six stretching, four bending and two umbrella modes in the methyl group; and four stretching modes and two bending modes in the amino group in four sets of coordinates NC, LNM, LC and OC are shown in the Figure A.13, A.14, A.15 and A.16 in the order. In this case, the vibrational motions of amino and methyl groups are well separated in all sets of coordinates. Notedly, the vibrational motions were localized on each methylamine monomer in both NC and LNM for amino group, while in LC and OC, all the stretching modes were localized on the hydrogen bonds and bending like motions localized on the functional groups.

The spectra simulated by VCI method with four sets of coordinates in N-H stretching region are shown in Figure 5.7 and the spectra in C-H stretching region are shown in Figure 5.8. In the N-H stretching region, NC, LNM, LC and OC gave similar results. The spectra simulated by VCI method with only three degrees of freedom of amino group of proton-donor methylamine gave very good agreement with the spectra simulated by six degrees of freedom. The small peaks at 3386 cm^{-1} and 3466 cm^{-1} in the six dimensional calculations comes from the stretching fundamental transitions of the amino group of proton-acceptor methylamine. In the C-H stretching region, the twelve dimensional spectra simulated by four sets of coordinates were very similar. However, the spectra features are more complicated and were not very well described by only six dimensional calculations on the methyl group of the proton-donor methylamine. The other bands can be recovered by

doi:10.6342/NTU202201978

including the other six degrees of freedom of the methyl group of the proton-acceptor methylamine. It is because two methyl groups are not identical but have negligible couplings.

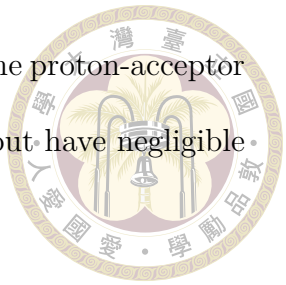

5.3.2.2 Methylamine trimer

For methylamine trimer molecule, nine and eighteen vibrational motions were considered for the amino and methyl groups, respectively.

The visualization of nine stretching, six bending and three umbrella modes in the methyl group in four sets of coordinates are shown in the Figure A.17, A.19, A.21 and A.23 ; and six stretching modes and four bending modes in the amino group are shown in the Figure A.18, A.20, A.22 and A.24. The vibrational motions of amino and methyl groups were still well separated in all sets of coordinates. However, unlike the methylamine dimer molecule, in methylamine trimer, the vibrational motions of each functional group were delocalized for the whole molecule in NC, while they were localized on each monomer in LNM, and even more localized on each hydrogen bond for the stretching motions in LC and OC.

Figure 5.9 and Figure 5.10 show the VCI calculated spectra in four different sets of coordinates in the N-H and C-H stretching region. In Figure 5.9, the spectra simulated by VCI method with three modes on the amino group of a methylamine monomer were capable to describe the main features of the spectra simulated with nine degrees of freedom. It is worthwhile to notice that the three dimensional calculations in two monomers gave very similar results, indicating that those two monomers had similar inter and intra molecular interactions. The spectra simulated

doi:10.6342/NTU202201978

by VCI method using six degrees of freedom on the methyl group of a methylamine monomer were also comparable with those results using eighteen degrees of freedom.

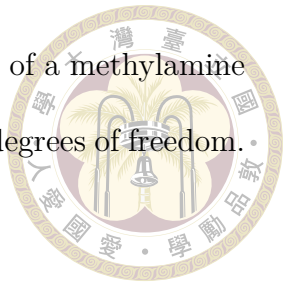

5.3.3 Lower-frequency motions

In addition, the rocking motions of methylamine dimer and trimer were also examine in four sets of coordinates. The frequencies and vibrational motions of the rocking modes in four sets of coordinates are shown in the Figure A.25 for dimer and in the Figure A.26 for trimer. In the methylamine dimer case, LNM and OC gave similar results for the rocking modes, with the motions were localized on each monomer and the frequencies did not change compared to NC. In LC, the mode vectors were also localized on each methylamine monomer, however, the frequencies of the proton-donor methylamine vibrations were different from NC by 27 cm^{-1}, indicating an over-localization happened. In the case of methylamine trimer, the mode vectors of the rocking motions were localized on each methylamine monomer in both LNM and LC, however, the LC frequencies deviated quite substantially from NC while LNM frequencies did not change much compared to NC's. OC tried to localize the motions of rocking modes with the frequencies changed within 1 cm^{-1} from the NC only. Noted that the mode vectors in OC were not fully localized compared to LNM and LC, but also not fully delocalized as in NC.

doi:10.6342/NTU202201978

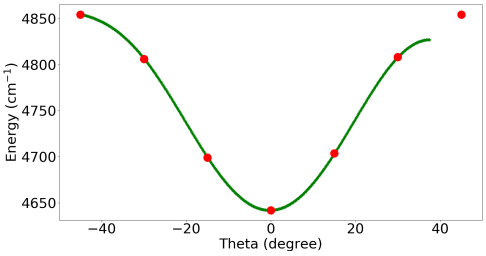

(a) $\tilde{E}_{1D}(\tilde{\theta}_{12})$

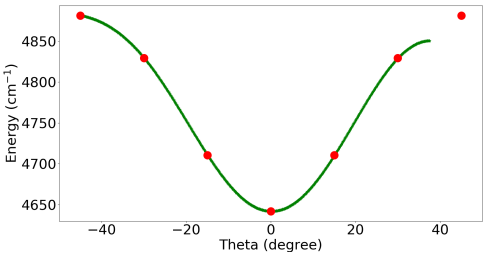

(b) $\tilde{E}_{1D}(\tilde{\theta}_{13})$

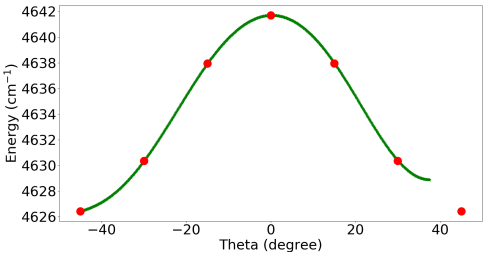

(c) $\tilde{E}_{1D}(\tilde{\theta}_{23})$

Figure 5.1: The energy is one-dimensional function of theta.. The red points were the scanning points of the one-dimensional energy function and the green points were the fitting points to the discrete cosine transforms.

doi:10.6342/NTU202201978

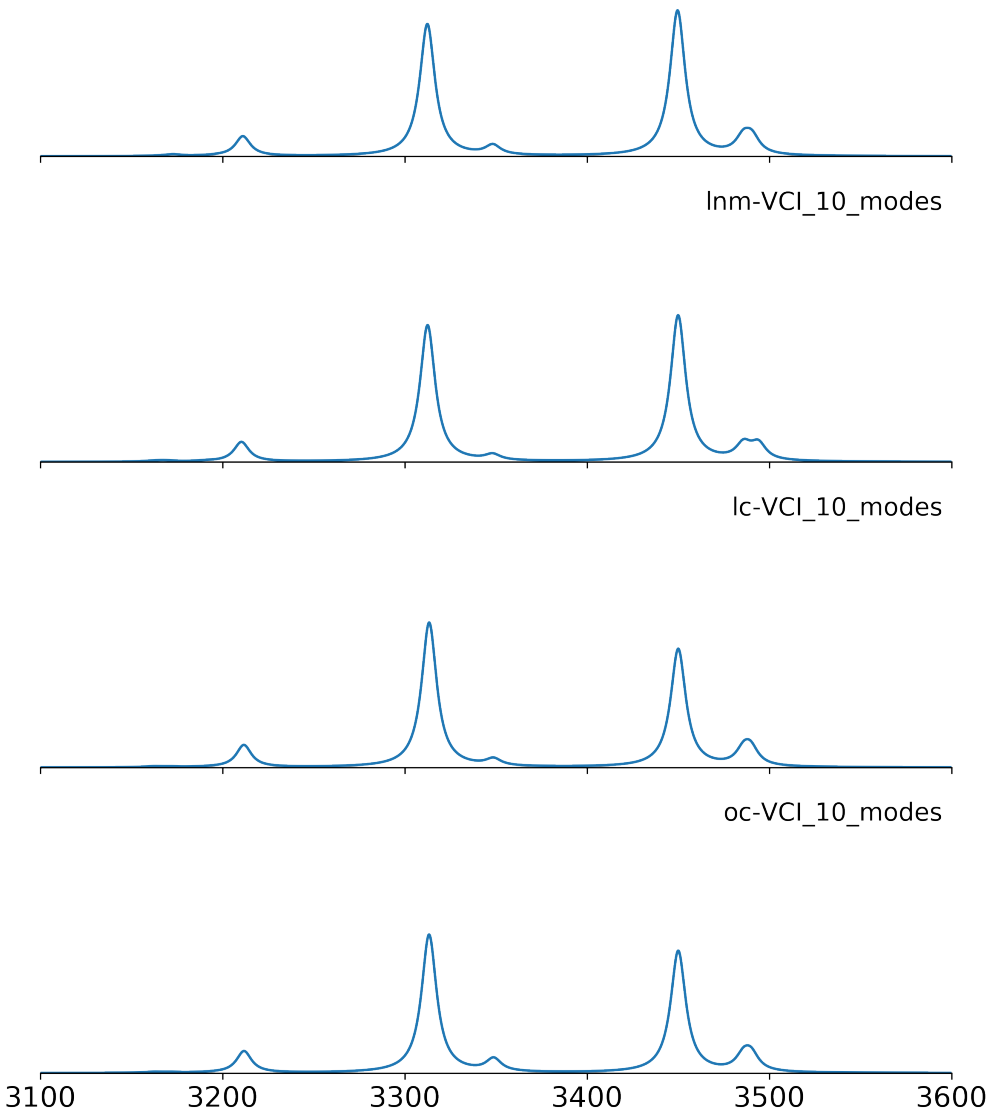

Figure 5.2: Spectra of ammonia dimer simulated by VCI method with NC, LNM, LC and OC using ten degrees of freedom.

doi:10.6342/NTU202201978

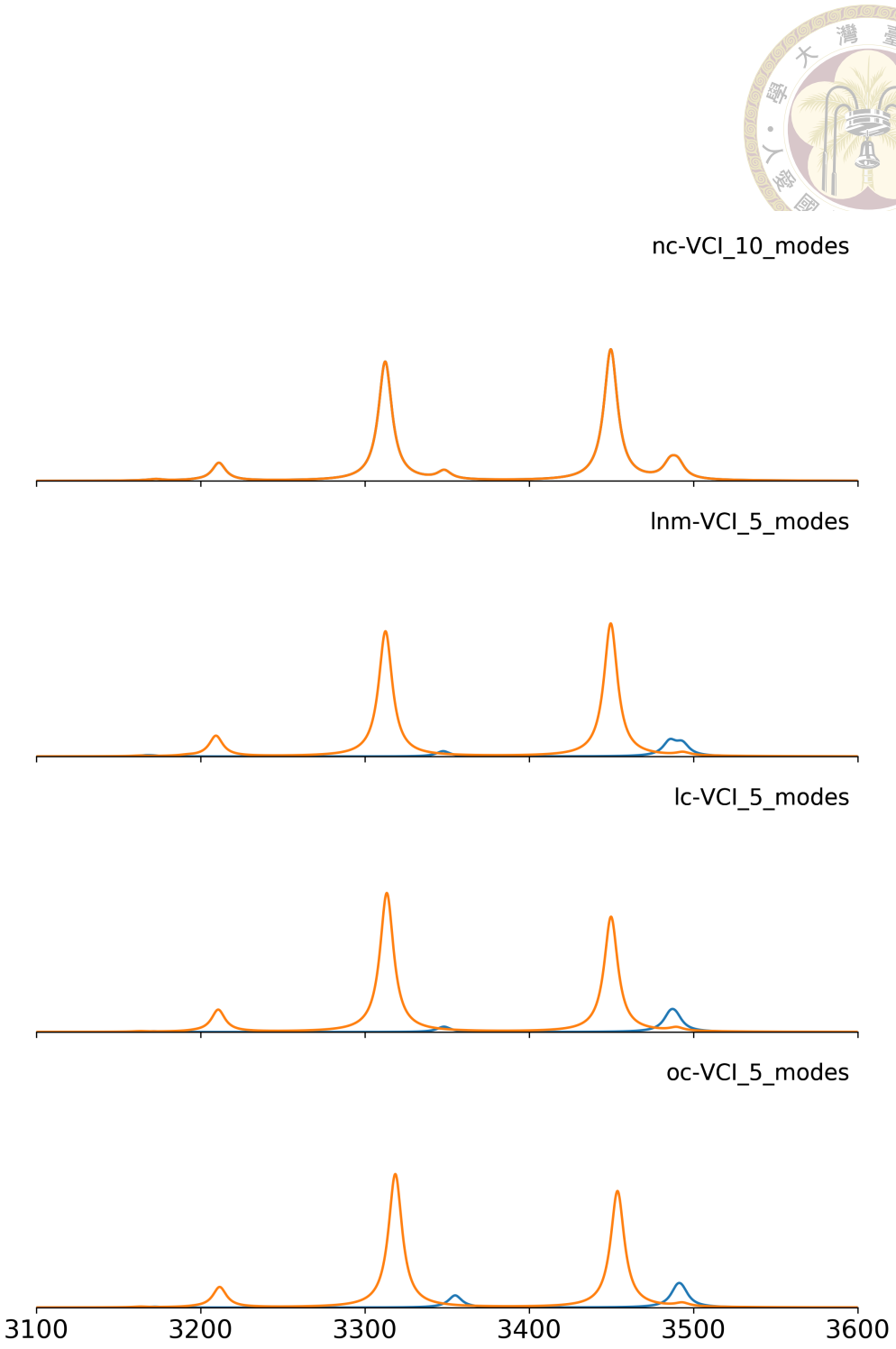

Figure 5.3: Spectra of ammonia dimer simulated by VCI method with NC using ten degrees of freedom, and with LNM, LC and OC using five degrees of freedom. The spectra in orange are the results of five-dimensional calculations on proton-donor. The spectra in blue are the results of five-dimensional calculations on proton-acceptor.

doi:10.6342/NTU202201978

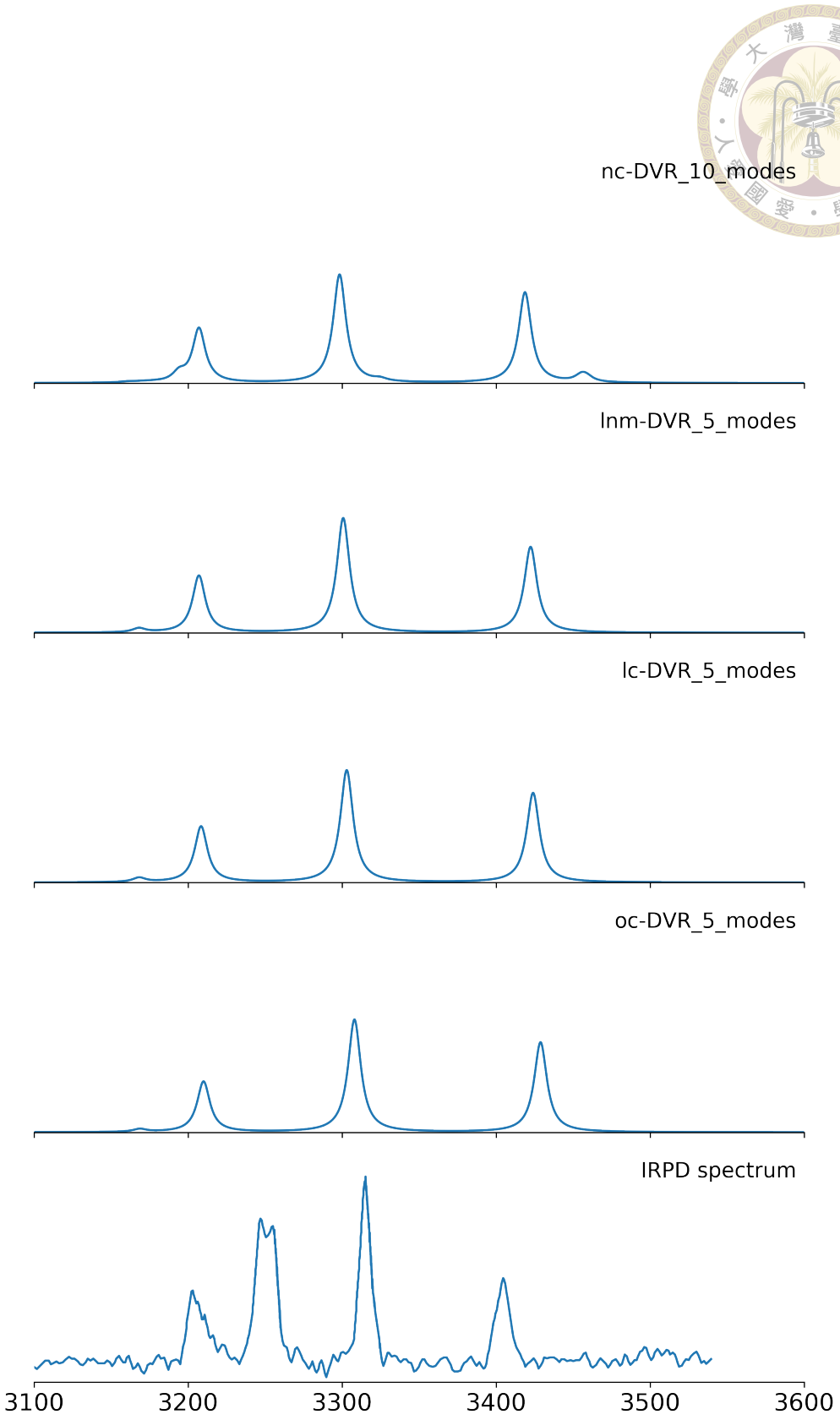

Figure 5.4: Spectra of ammonia dimer simulated by DVR method with NC using ten degrees of freedom, and with LNM, LC and OC using five degrees of freedom.

doi:10.6342/NTU202201978

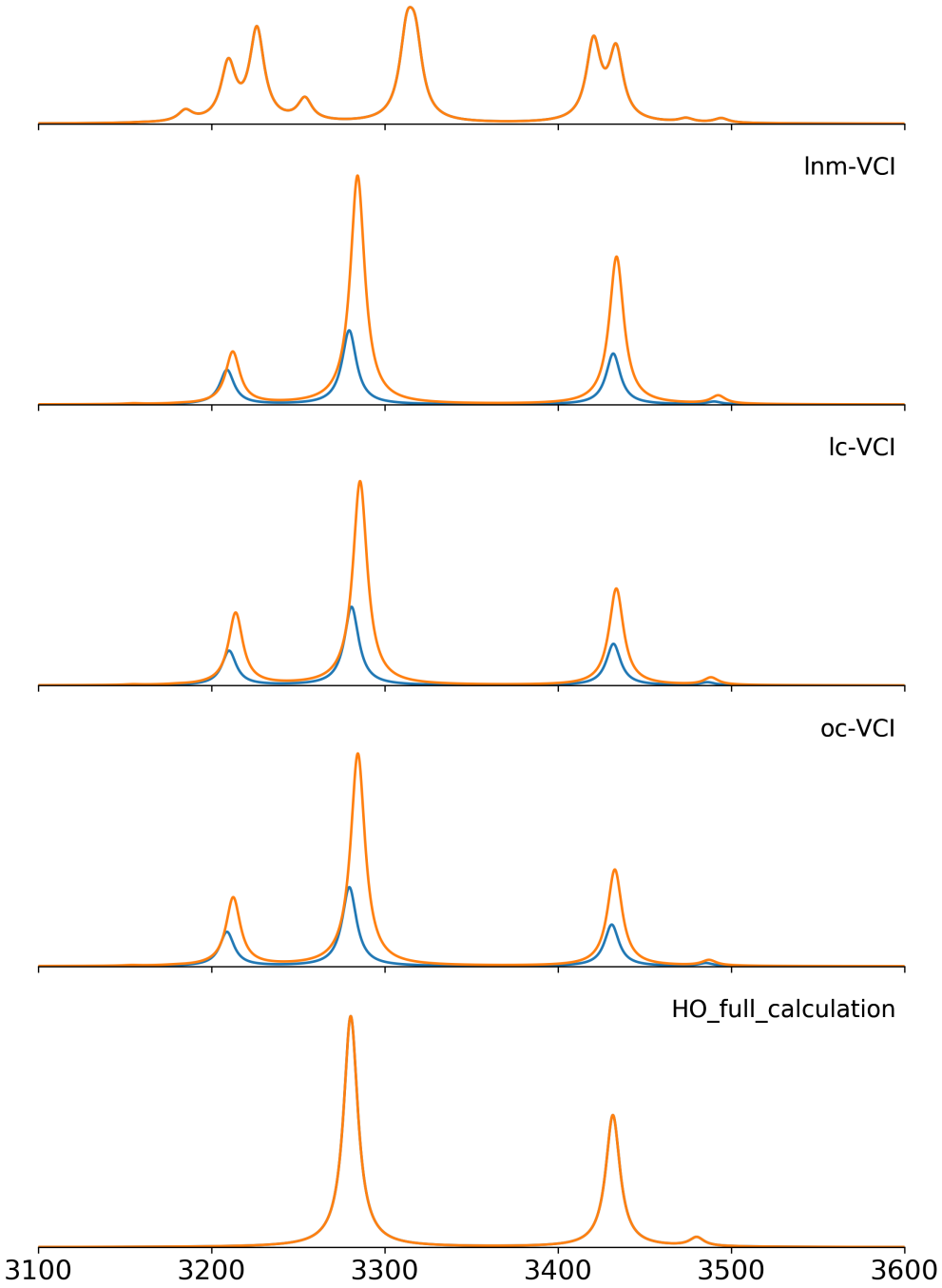

Figure 5.5: Spectra of ammonia trimer simulated by VCI method with NC, LNM, LC and OC. The spectra in orange are the results of fifteen dimensional calculations. The spectra in blue are the results of five dimensional calculations on an ammonia monomer.

doi:10.6342/NTU202201978

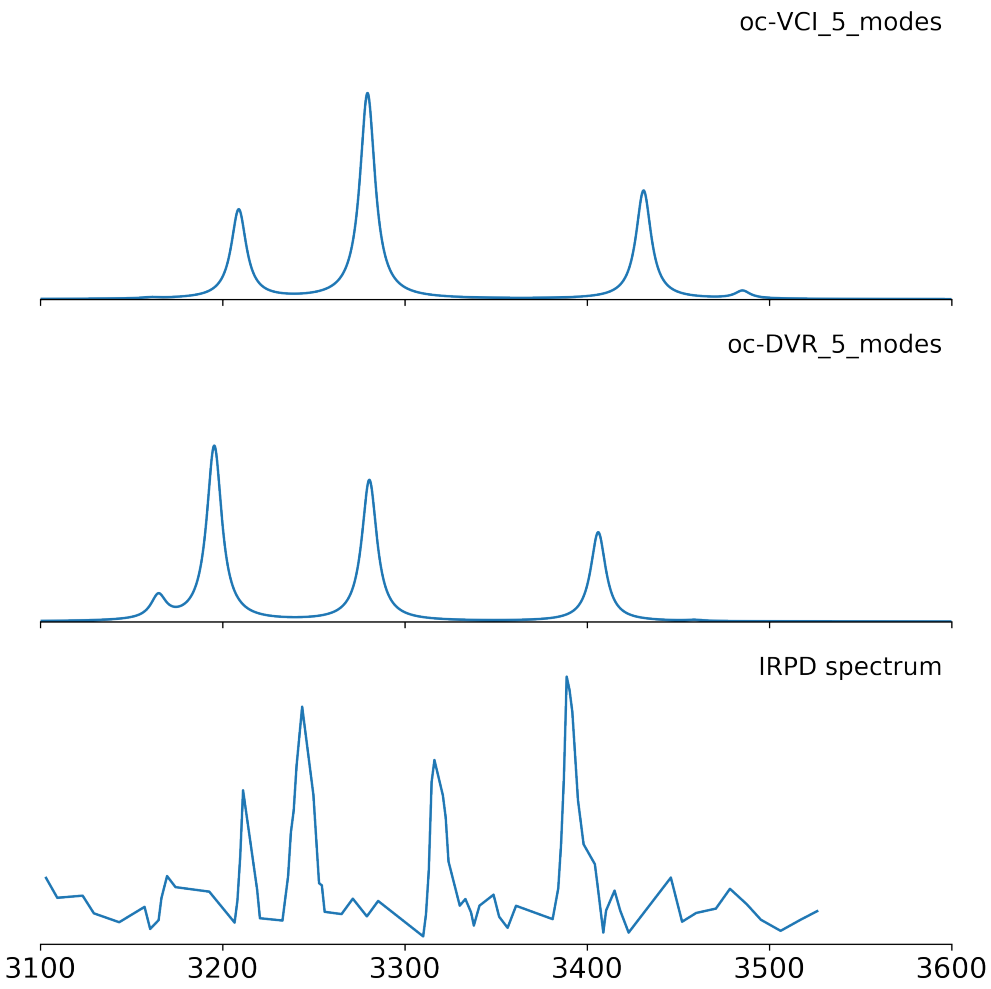

Figure 5.6: Spectra of ammonia trimer simulated by VCI and DVR with five degrees of freedom on an ammonia monomer in OC and compared to the experimental spectrum.

doi:10.6342/NTU202201978

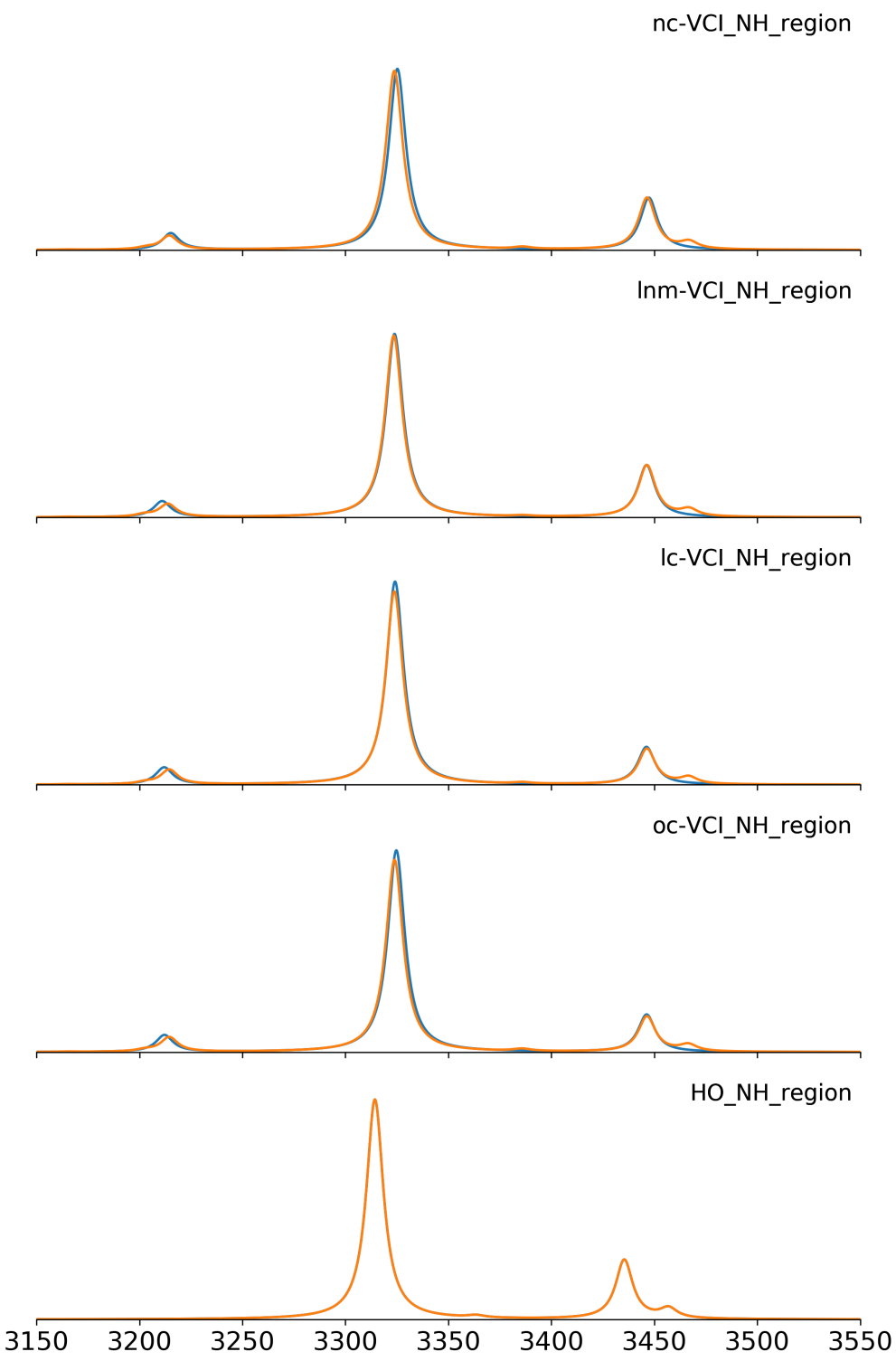

Figure 5.7: Spectra of methylamine dimer in NH stretching region simulated by VCI method with NC, LNM, LC and OC and compared to the harmonic calculation. The spectra in orange are the results of six dimensional calculations on the amino group of both monomers. The spectra in blue are the results of three dimensional calculations on the amino group of the proton-donor monomer.

doi:10.6342/NTU202201978

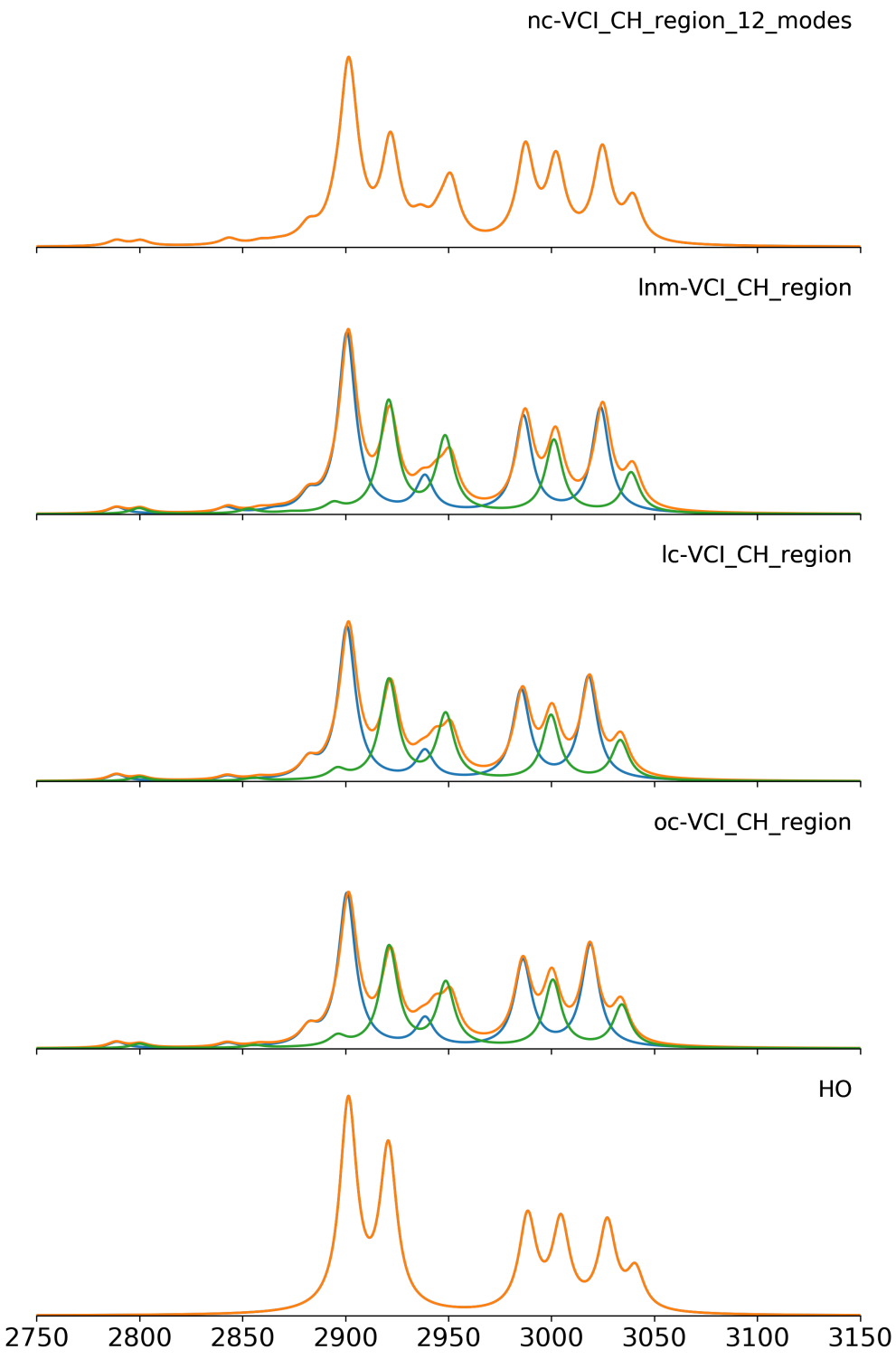

Figure 5.8: Spectra of methylamine dimer in CH stretching region simulated by VCI method with NC, LNM, LC and OC and compared to the harmonic calculation. The spectra in orange are the results of twelve dimensional calculations on the methyl group of both monomers. The spectra in blue and in green are the results of six dimensional calculations on the methyl group of the proton-donor and proton-acceptor methylamine, respectively.

doi:10.6342/NTU202201978

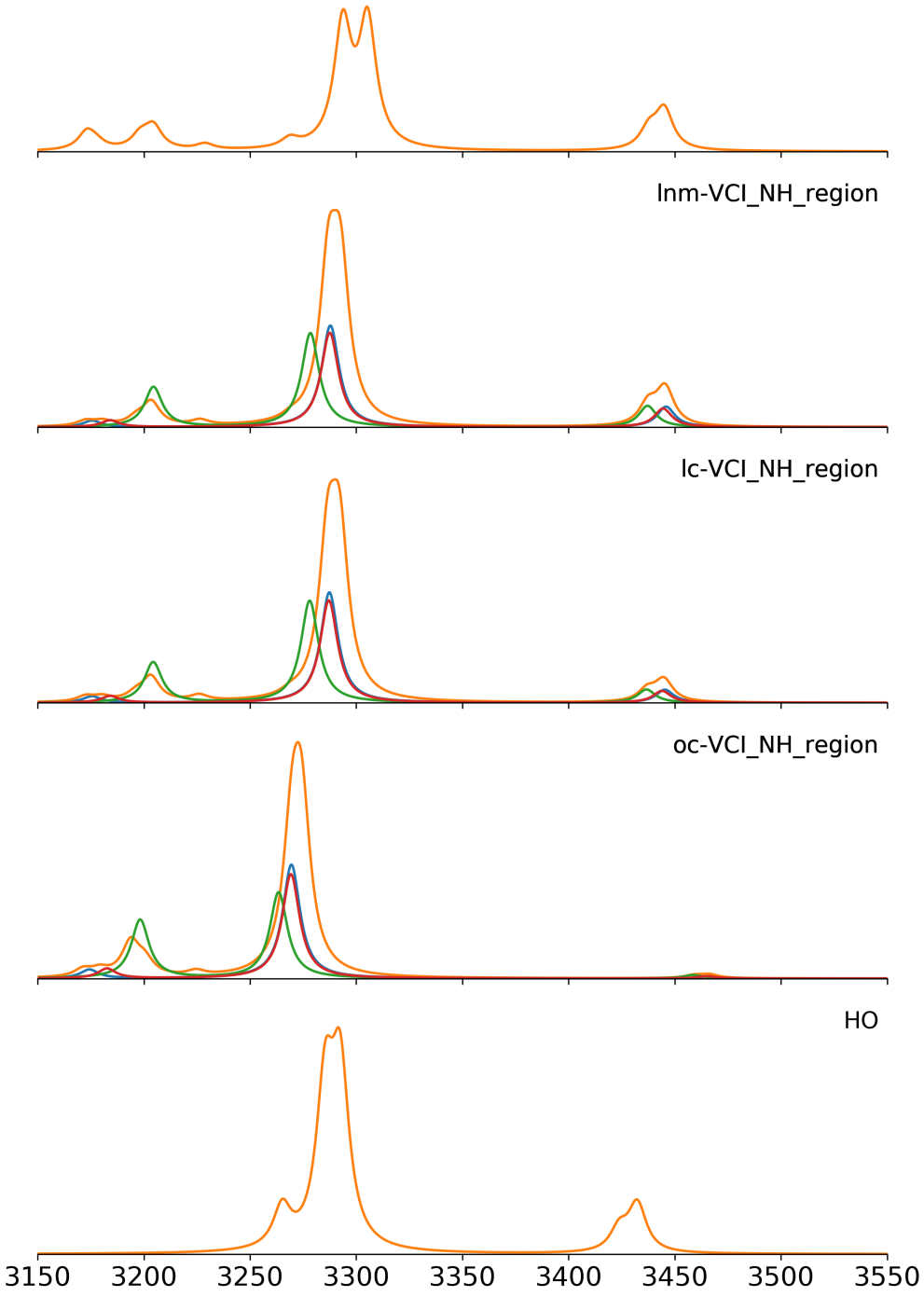

Figure 5.9: Spectra of methylamine trimer in NH stretching region simulated by VCI method with NC, LNM, LC and OC and compared to the harmonic calculation. The spectra in orange are the results of nine dimensional calculations. The spectra in blue, green and purple are the results of three dimensional calculations on the amino group of each methylamine monomer.

doi:10.6342/NTU202201978

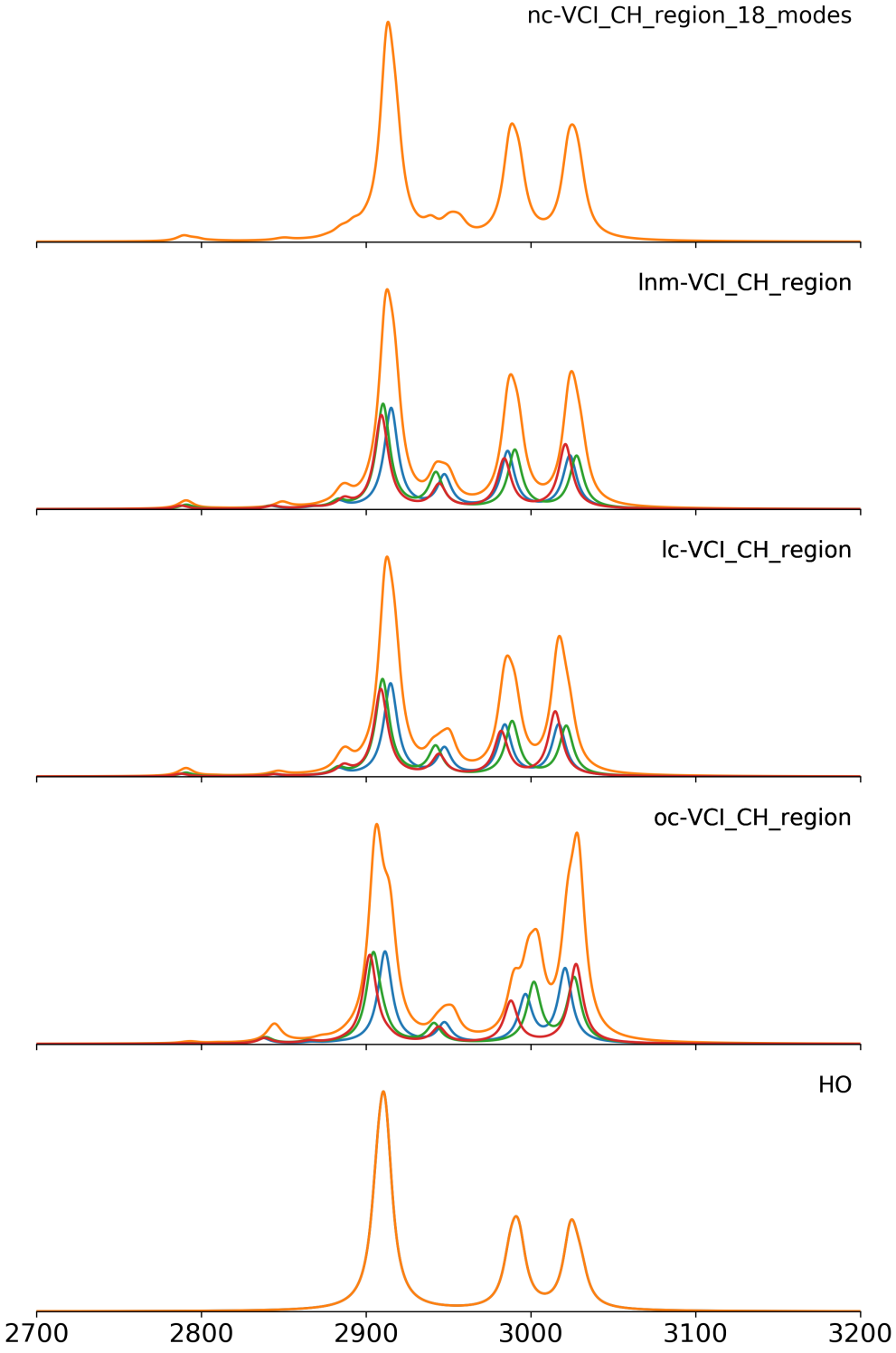

Figure 5.10: Spectra of methylamine trimer in CH stretching region simulated by VCI method with NC, LNM, LC and OC and compared to the harmonic calculation. The spectra in orange are the results of eighteen dimensional calculations. The spectra in blue, green and purple are the results of six dimensional calculations on the methyl group of each methylamine monomer.

doi:10.6342/NTU202201978

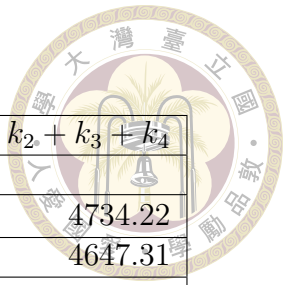

		k_2	k_2+k_3	k_2+k_4	$k_2+k_3+k_4$
H2O monomer					
HO	$\langle 0\|\hat{H}\|0\rangle$	4681.57	4681.57	4734.22	4734.22
	E_{GS}	4681.57	4591.31	4734.22	4647.31
FBR	$\langle 0\|\hat{H}\|0\rangle$	4681.57	4597.41	4731.62	4659.65
	E_GS	4681.57	4573.72	4731.62	4641.69
H2O dimer					
HO	$\langle 0\|\hat{H}\|0\rangle$	9297.82	9297.82	9405.76	9405.76
	E_{GS}	9297.82	9115.21	9405.76	9229.82
FBR	$\langle 0\|\hat{H}\|0\rangle$	9297.82	9085.55	9399.88	9227.88
	E_GS	9297.82	9055.56	9399.88	9204.64
NH3 dimer					
HO	$\langle 0\|\hat{H}\|0\rangle$	14015.17	14015.17	14126.08	14126.08
	E_{GS}	14015.17	13788.49	14126.08	13906.31
FBR	$\langle 0\|\hat{H}\|0\rangle$	14015.17	13861.76	14121.29	13984.12
	E_{GS}	14015.17	13750.77	14121.29	13889.79
NH3 trimer					
HO	$\langle 0\|\hat{H}\|0\rangle$	14015.17	14015.17	14126.08	14126.08
	E_{GS}	14015.17	13788.49	14126.08	13906.31
FBR	$\langle 0\|\hat{H}\|0\rangle$	14015.17	13861.76	14121.29	13984.12
	E_{GS}	14015.17	13750.77	14121.29	13889.79
MMA dimer					
HO	$\langle 0\|\hat{H}\|0\rangle$	25040.93	25040.93	25068.31	25068.31
	E_{GS}	25040.93	24782.52	25068.31	24815.15
FBR	$\langle 0\|\hat{H}\|0\rangle$	25040.93	24756.92	25064.27	24817.12
	E_{GS}	25040.93	24708.81	25064.27	24773.82

Table 5.1: The ground state energy in normal mode coordinates in HO and FBR basis before and after diagonalizing the CI matrix, which are denoted as $\langle 0|\hat{H}|0\rangle$ and E_{GS} respectively. All the energies are shown in cm^{-1}. k_2, k_3, and k_4 are the harmonic, cubic and quartic terms of the potential energy surfaces.

sweep	E_{GS}	ΔE_{GS}	θ_{12}	θ_{13}	θ_{23}
0	4641.6896	0	0	0	0
1	4626.4698	15.2198	-0.4377	0.0000	-45.0000
2	4626.4248	0.0450	0.2512	0.2512	0.0000
3	4626.4247	$5.94\text{x}10^{-05}$	0.0091	0.0091	-0.0005

Table 5.2: Jacobi sweeps for water molecule. The energies are in cm^{-1}, and the theta are in degree.

doi:10.6342/NTU202201978

	Normal mode coordinates	Optimized coordinates
	Diagonal matrix elements	
f_{22}	3803.31	3871.00
f_{222}	1830.39	2569.67
f_{2222}	325.67	453.19
f_{33}	3937.53	3871.00
f_{333}	0	2569.67
f_{3333}	0	453.19
	Off-diagonal matrix elements	
f_{23}	0	-134.21
f_{233}	1813.8	-16.31
f_{223}	0	-16.31
f_{2333}	317.17	-2.88
f_{2233}	0	-2.88
f_{2223}	0	-2.88

Table 5.3: The second-order, third-order and forth-order force constants of two stretching modes of the water monomer molecule in normal mode coordinates and optimized coordinates. All the values are shown in cm^{-1}.

doi:10.6342/NTU202201978

	nc-VCI[3]-(2)		nc-VCI[1]-(8)		nc-VCI[2]-(8)		nc-VCI[3]-(8)
E_{GS}	4645.94	21.80	4639.88	15.74	4624.21	0.07	4624.14
ν_1	1561.33	10.73	1621.6	71	1567.52	16.92	1550.60
ν_2	3715.62	52.58	3683.35	20.31	3664.22	1.18	3663.04
ν_3	3827.38	50.27	4169.19	392.08	3779.21	2.1	3777.11
$2\nu_1$	3148.77	78.18	3126.71	56.12	3089.56	18.97	3070.59
$\nu_1\nu_2$	5567.66	403.87			5201.86	38.07	5163.79
$\nu_1\nu_3$	5617.63	366.82			5607.76	356.95	5250.81
$2\nu_2$	8667.70	1370.43	7338.79	41.52	7299.65	2.38	7297.27
$\nu_2\nu_3$	8660.34	1261.38			7426.42	27.46	7398.96
$2\nu_3$	8209.02	684.82	8409.67	885.47	7534.79	10.59	7524.20
MAD		430.09		148.22		47.47	

	oc-VCI[3]-(2)		oc-VCI[1]-(8)		oc-VCI[2]-(8)		oc-VCI[3]-(8)
E_{GS}	4646.02	21.96	4628.47	4.41	4624.25	0.19	4624.06
ν_1	1560.34	10.67	1632.14	82.47	1552.90	3.23	1549.67
ν_2	3764.68	101.64	3737.94	74.90	3663.20	0.16	3663.04
ν_3	3786.76	9.65	3829.95	52.84	3778.00	0.89	3777.11
$2\nu_1$	3146.52	75.93	3138.79	68.2	3072.60	2.01	3070.59
$\nu_1\nu_2$	5549.15	385.36			5243.20	79.41	5163.79
$\nu_1\nu_3$	5628.77	377.96			5264.8	13.99	5250.81
$2\nu_2$	8707.38	1410.11	7475.40	178.13	7303.20	5.93	7297.27
$\nu_2\nu_3$	8152.29	753.33			7399.30	0.34	7398.96
$2\nu_3$	8653.65	1129.45	7476.25	-47.95	7545.50	21.30	7524.20
MAD		427.61		41.30		12.74	

Table 5.4: The ground-state energy and the first few eigenvalues in the VCI calculations with normal mode coordinates and optimized coordinates for water monomer molecule. The energies are shown in cm^{-1}. The notation VCI[m]-(n) with m is the number of modes that are simultaneously excited, and n is the maximum sum of quantum numbers. Considering VCI[3]-(8) as the full calculation, the deviations of those truncated-basis set calculations and the mean absolute deviations from the full calculation are shown in the parentheses.

doi:10.6342/NTU202201978

nc-DVR	$\|0,0,0\rangle$	$\|1,0,0\rangle$	$\|0,1,0\rangle$	$\|0,0,1\rangle$	$\|2,0,0\rangle$	$\|0,2,0\rangle$	$\|0,0,2\rangle$
$\|0,0,0\rangle$	0.00	48.86	-252.64	0	45.91	58.25	-39.26
$\|1,0,0\rangle$	48.86	1552.08	15.14	0	-58.45	9.13	54.97
$\|0,1,0\rangle$	-252.64	15.14	3686.81	0	-78.93	-346.33	-433.64
$\|0,0,1\rangle$	0	0	0	3976.02	0	0	0
$\|2,0,0\rangle$	45.91	-58.45	-78.93	0	3100.71	42.63	47.22
$\|0,2,0\rangle$	58.25	9.13	-346.33	0	42.63	7308.03	123.08
$\|0,0,2\rangle$	-39.26	54.97	-433.64	0	47.22	123.08	8042.24
oc-DVR	$\|0,0,0\rangle$	$\|1,0,0\rangle$	$\|0,1,0\rangle$	$\|0,0,1\rangle$	$\|2,0,0\rangle$	$\|0,2,0\rangle$	$\|0,0,2\rangle$
$\|0,0,0\rangle$	0.00	52.51	20.52	20.33	33.81	-24.68	-24.60
$\|1,0,0\rangle$	52.51	1569.80	17.67	17.67	-69.55	25.17	25.15
$\|0,1,0\rangle$	20.52	17.67	3687.77	-63.46	-45.21	25.85	10.73
$\|0,0,1\rangle$	20.33	17.67	-63.46	3687.71	-45.25	10.44	25.60
$\|2,0,0\rangle$	33.81	-69.55	-45.21	-45.25	3134.77	40.17	40.18
$\|0,2,0\rangle$	-24.68	25.17	25.85	10.44	40.17	7267.85	-1.43
$\|0,0,2\rangle$	-24.60	25.15	10.73	25.60	40.18	-1.43	7267.71

Table 5.5: Hamiltonian matrix elements in DVR calculations for water monomer molecule. The energies are shown in cm^{-1}. The ground state energies were 4617.07 and 4617.26 cm^{-1} for the calculations with normal mode coordinates and optimized coordinates respectively. All the diagonal elements were subtracted by the ground state energies. The off-diagonal matrix elements are the coupling between the basis kets.

nc-DVR	Peak position	Intensity	Assignment	Projection^2
	0	0	$\langle 0\|0.0.0\rangle$	99.18%
	1559.48	90.14	$\langle 1\|1.0.0\rangle$	99.20%
	3094.46	0.47	$\langle 2\|2.0.0\rangle$	97.33%
	3627.51	10.90	$\langle 3\|0.1.0\rangle$	94.75%
	3736.23	70.79	$\langle 4\|0.0.1\rangle$	92.84%
oc-DVR	Peak position	Intensity	Assignment	Projection^2
	0	0	$\langle 0\|0.0.0\rangle$	99.83%
	1559.48	90.15	$\langle 1\|1.0.0\rangle$	99.40%
	3094.48	0.47	$\langle 2\|2.0.0\rangle$	97.04%
	3628.58	10.90	$\langle 3\|0.0.1\rangle$	48.98%
			$\langle 3\|0.1.0\rangle$	48.93%
	3738.16	70.86	$\langle 4\|0.1.0\rangle$	49.55%
			$\langle 4\|0.0.1\rangle$	49.50%

Table 5.6: DVR calculations with normal mode coordinates and optimized coordinates for water monomer molecule. The peak positions are in cm^{-1}. The peak intensities are in KM/Mole unit. The projection^2 were obtained by the inner product between the eigenstates and the basis kets.

doi:10.6342/NTU202201978

	Normal mode coordinates	Optimized coordinates
	Diagonal matrix elements	
f_{99}	3704.26	3725.14
f_{1010}	3795.73	3860.44
f_{1111}	3904.28	3884.91
f_{1212}	3924.67	3860.48
f_{999}	2293.04	2646.21
f_{101010}	-1803.27	-2569.91
f_{111111}	-2049.66	-2573.66
f_{121212}	-4.28	-2570.10
	Off-diagonal matrix elements	
f_{910}	0	11.43
f_{911}	0	119.12
f_{912}	0	11.31
f_{1011}	0	0.38
f_{1012}	0	-129.49
f_{1112}	0	0.36
f_{91010}	174.06	6.68
f_{9910}	166.47	2.09
f_{91111}	1041.46	39.83
f_{9911}	512.00	73.96
f_{91212}	162.02	7.81
f_{9912}	-0.26	3.24
f_{101111}	138.92	1.39
f_{101011}	-46.18	-1.60
f_{101212}	-1807.11	18.74
f_{101012}	1.37	15.40
f_{111212}	0.67	0.24
f_{111112}	-42.92	-0.43
f_{91011}	20.63	0.00
f_{91012}	-0.21	-1.50
f_{91112}	-0.35	0.06
f_{101112}	-0.68	-0.16

Table 5.7: The second and third order force constants of four stretching modes of the water dimer molecule in normal mode coordinates and optimized coordinates. All values are shown in cm^{-1}.

doi:10.6342/NTU202201978

	nc-VCI[3]-(4)		nc-VCI[3]-(5)		nc-VCI[4]-(5)		nc-VCI[3]-(6)		nc-VCI[6]-(6)
H size	791^2		1701^2		2751^2		3136^2		8008^2
(H size)/(H[6]-(6) size)	0.98 %		4.51 %		11.80 %		15.34 %		
ZPE	13835.47	1.84	13834.96	1.33	13834.19	0.56	13834.61	0.98	13833.63
9	1593.73	12.44	1589.97	8.67	1582.10	0.81	1589.97	8.67	1581.29
10	1602.78	12.60	1599.07	8.89	1591.01	0.83	1599.04	8.86	1590.18
11	1607.13	12.47	1603.36	8.70	1595.48	0.81	1603.37	8.71	1594.66
12	1627.28	12.61	1623.52	8.84	1615.50	0.82	1623.49	8.81	1614.68
13	3347.99	36.05	3321.67	9.72	3315.52	3.57	3319.06	7.11	3311.94
14	3375.93	28.21	3356.07	8.34	3350.48	2.76	3354.31	6.59	3347.72
15	3473.90	25.01	3459.89	11.01	3451.41	2.53	3458.81	9.93	3448.89
16	3508.79	23.77	3495.92	10.90	3487.33	2.31	3494.92	9.90	3485.02
17	3510.49	20.52	3497.83	7.86	3491.97	2.00	3497.05	7.08	3489.97
18	3510.99	20.83	3498.49	8.33	3492.16	2.01	3497.70	7.55	3490.16
MAD		(18.76)		(8.42)		(1.73)		(7.65)	

Table 5.8: The ground-state energy and the first few eigenvalues in the VCI calculations with normal mode coordinates for ammonia dimer molecule. The energies are shown in cm^{-1}. The notation VCI[m]-(n) with m is the number of modes that are simultaneously excited, and n is the maximum sum of quantum numbers. The mean absolute deviations from the larger basis set calculation VCI[6] − (6) are shown in the parentheses.

doi:10.6342/NTU202201978

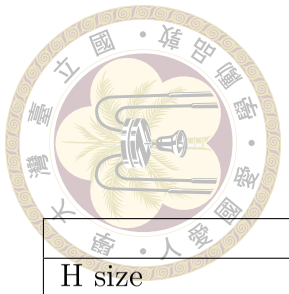

	oc-VCI[3]-(4)		oc-VCI[3]-(5)		oc-VCI[4]-(5)		oc-VCI[3]-(6)		oc-VCI[6]-(6)
H size	791^2		1701^2		2751^2		3136^2		8008^2
(H size)/(H[6]-(6) size)	0.98		4.51		11.80		15.34		
ZPE	13835.80	1.42	13835.01	0.63	13834.92	0.53	13834.50	0.12	13834.38
9	1589.65	8.03	1583.58	1.96	1582.11	0.49	1583.36	1.74	1581.62
10	1598.57	8.02	1592.50	1.96	1591.02	0.47	1592.30	1.75	1590.55
11	1602.89	7.96	1596.84	1.91	1595.39	0.46	1596.64	1.71	1594.93
12	1623.12	8.03	1617.03	1.94	1615.57	0.48	1616.82	1.72	1615.09
13	3346.49	33.27	3318.12	4.91	3317.01	3.80	3314.60	1.39	3313.21
14	3375.53	26.88	3353.44	4.79	3351.49	2.85	3350.99	2.34	3348.65
15	3471.05	21.07	3453.23	3.26	3452.21	2.23	3451.12	1.15	3449.97
16	3505.64	19.78	3489.18	3.32	3487.92	2.06	3487.32	1.46	3485.86
17	3510.17	20.27	3493.56	3.66	3492.00	2.09	3491.69	1.78	3489.90
18	3510.37	20.33	3493.76	3.73	3492.13	2.09	3491.97	1.93	3490.04
MAD		(15.91)		(2.91)		(1.60)		(1.55)	

Table 5.9: The ground-state energy and the first few eigenvalues in the VCI calculations with optimized coordinates for ammonia dimer molecule. The energies are shown in cm^{-1}. The notation VCI[m]-(n) with m is the number of modes that are simultaneously excited, and n is the maximum sum of quantum numbers. The mean absolute deviations from the larger basis set calculation VCI[6] − (6) are shown in the parentheses.

	lc-VCI[3]-(4)		lc-VCI[3]-(5)		lc-VCI[4]-(5)		lc-VCI[3]-(6)		lc-VCI[6]-(6)
H size	791^2		1701^2		2751^2		3136^2		8008^2
(H size)/(H[6]-(6) size)	0.98		4.51		11.80		15.34		
ZPE	13835.81	1.42	13835.00	0.62	13834.92	0.53	13834.49	0.10	13834.38
9	1589.59	7.99	1583.46	1.86	1582.09	0.49	1583.23	1.63	1581.60
10	1598.58	7.97	1592.44	1.83	1591.08	0.47	1592.22	1.61	1590.61
11	1602.89	7.92	1596.77	1.81	1595.43	0.46	1596.57	1.60	1594.97
12	1623.05	8.01	1616.91	1.86	1615.52	0.48	1616.69	1.64	1615.04
13	3346.75	33.49	3318.49	5.24	3317.08	3.82	3315.01	1.75	3313.26
14	3375.12	26.55	3352.75	4.18	3351.43	2.86	3350.15	1.58	3348.57
15	3471.12	21.15	3453.30	3.33	3452.22	2.24	3451.20	1.23	3449.97
16	3505.56	19.66	3489.06	3.16	3487.96	2.06	3487.14	1.24	3485.90
17	3509.90	20.28	3493.28	3.66	3491.73	2.10	3491.42	1.79	3489.63
18	3510.52	20.30	3493.85	3.64	3492.31	2.09	3492.00	1.78	3490.22
MAD		(15.89)		(2.83)		(1.60)		(1.45)	

Table 5.10: The ground-state energy and the first few eigenvalues in the VCI calculations with localized coordinates for ammonia dimer molecule. The energies are shown in cm^{-1}. The notation VCI[m]-(n) with m is the number of modes that are simultaneously excited, and n is the maximum sum of quantum numbers. The mean absolute deviations from the larger basis set calculation VCI[6] − (6) are shown in the parentheses.

doi:10.6342/NTU202201978

Wavenumber	Intensity	Assignment	Projection^2	μ_x	μ_y	μ_z
3467.182	0.016	<8|0.0.0.0.1>	48.58%	0	0.001	-0.008
		<8|0.0.0.1.0>	48.54%	0	0.001	0.008
		<8|1.1.0.0.0>	2.53%	0	-0.001	0

Table 5.11: The projection of the intensity of the band at 3467 cm^{-1}. The five number on the kets are corresponding to the quantum number of five modes on the proton-donor ammonia. μ_x, μ_y and μ_z are the transition dipole moment projected on the basis kets.

doi:10.6342/NTU202201978

Chapter 6 Conclusion

We have implemented several algorithms to find the optimal set of coordinates: the localized coordinates based on the localization criterion of maximizing the sum of the squared of atomic contributions to the modes, proposed by Jacob and Reiher in 2009 [11]; and the optimized coordinates based on Thompson and Truhlar's idea in 1982 [15] of minimizing the ground state energy, and Yagi"s optimization algorithm proposed in 2012 [16]. However, in this thesis, a modification was made to calculate the ground state energy by finite basis representation method instead of VSCF. The Hamiltonian in FBR was written as the sum of one-mode Hamiltonian and the coupling of the modes, the ground state energy was obtained by diagonalizing the Hamiltonian matrix. This method was an improvement of VSCF because we can obtain the ground state energy without iterative processes. The optimization algorithm is based on the Jacobi sweep and the Newton's minimization. The many-variable optimization problem is simplified by defining the unitary transformation matrix as the product of Jacobi rotational matrices of one pair. The localization algorithm is also similar to the optimization algorithm, however, instead of maximizing localization criterion, we minimize its negative function.

Water monomer and dimer were choosen as the benchmark of the optimization process and the performance of optimized coordinates in VCI calculations. The total

doi:10.6342/NTU202201978

coupling constants in the cubic and quartic potentials of water monomer and dimer were smaller in optimized coordinates than in normal mode coordinates. The VCI calculations with truncated basis sets showed that optimized coordinates had faster convergence than normal mode coordinates did. From this result, VCI calculations with optimized coordinates could be used with smaller basis sets, which could help to save the computational time. The size of the basis sets could be chosen as five for the maximum quantum number and four for the number of simultaneously excited modes.

In this study, Fermi resonance patterns of ammonia and methylamine clusters spectra were study with four choices of coordinates, which are normal mode coordinates (NC), local normal mode coordinates (LNM), localized coordinates (LC) and optimized coordinates (OC). In both tested clusters, the vibrational motions were delocalized in NC but localized in LNM, LC and OC. In LNM, the vibrational modes were localized on each monomer due to the way we chose the fragments. The LC and OC gave similar results for bending and stretching motions, in which the stretching modes were localized on the hydrogen bonds and the bending modes localized on the functional groups. It would help to simplify the pictures of vibrational motions and reduce the number of degrees of freedom needed in VCI and DVR calculations when studying the properties of a chemical unit.

The examples of two hydrogen bonded clusters haven't reached to the boundaries of those localized/optimized techniques, therefore they gave us roughly similar results in the vibrational frequencies, coordinates and the simulated spectra. Only when we went to lower-frequency region of the rocking modes, the over-localization were found in LC, while the modes obtained by LNM and OC agreed reasonably

doi:10.6342/NTU202201978

well with the harmonic frequencies, making the results more reliable.

From our study and experience, LNM would be recommended for the molecules or clusters with the functional groups are weakly binded, i.e. the inter-molecular interactions are negligible so the systems can be easily divided into fragments. Only block-diagonalizations of the Hessian matrix is needed to obtain the frequencies and mode vectors, so LNM is very quick. The disadvantages of this method is it relies on our chemical intuition and cannot be applied on the strongly binded systems. LC also only needs the information of the Hessian matrix, and it is a more automatic way to localize the motions, therefore LC should be a good choice for the high frequency modes but not on the low frequency modes due to the over-localization. OC is an expensive method because it requires an anharmonic potential, but it also an "optimal choice" because it carries out the information of the anharmonic potential. OC would give similar results to LC when the inter-mode anharmonic coupling in NC is significant while the harmonic coupling introduced by OC is not too big. In the reverse way, OC would give similar results to NC when the potential is harmonic or nearly harmonic. Therefore, when studying a new system, the total anharmonic coupling constants and the harmonic coupling introduced by a rotational matrix should be considered to choose an "optimal" set of coordinates. For the future work, more research on the low-frequency region and aromatic molecules should be done to investigate the advantages of optimized coordinates over the localized coordinates and local normal mode coordinates, since in the aromatic molecules, there is no clear way to cut the rings into smaller fragments.

doi:10.6342/NTU202201978

doi:10.6342/NTU202201978

References

[1] W. Demtröder, *Molecular Physics: Theoretical Principles and Experimental Methods*, Physics textbook (Wiley, 2008).

[2] P. T. Panek and C. R. Jacob, The Journal of Chemical Physics **144**, 164111 (2016).

[3] J. D. Head, V. Kairys, and Y. Shi, Journal of Molecular Structure: THEOCHEM **464**, 153 (1999).

[4] Q.-R. Huang, Y. Matsuda, R. Eguchi, A. Fujii, and J. Kuo, Journal of the Chinese Chemical Society **69**, 42 (2022).

[5] Q.-R. Huang, R. Shishido, C.-K. Lin, C.-W. Tsai, J. A. Tan, A. Fujii, and J.-L. Kuo, Angewandte Chemie International Edition **60**, 1936 (2021).

[6] Q.-R. Huang, T. Endo, S. Mishra, B. Zhang, L.-W. Chen, A. Fujii, L. Jiang, G. N. Patwari, Y. Matsuda, and J.-L. Kuo, Physical Chemistry Chemical Physics **23**, 3739 (2021).

[7] B. Zhang, S. Yang, Q.-R. Huang, S. Jiang, R. Chen, X. Yang, D. H. Zhang, Z. Zhang, J.-L. Kuo, and L. Jiang, CCS Chemistry **3**, 829 (2021).

doi:10.6342/NTU202201978

[8] S. Mishra, H.-Q. Nguyen, Q.-R. Huang, C.-K. Lin, J.-L. Kuo, and G. N. Patwari, The Journal of Chemical Physics **153**, 194301 (2020).

[9] C.-K. Lin, Q.-R. Huang, and J.-L. Kuo, Physical Chemistry Chemical Physics **22**, 24059 (2020).

[10] C.-K. Lin, R. Shishido, Q.-R. Huang, A. Fujii, and J.-L. Kuo, Physical Chemistry Chemical Physics **22**, 22035 (2020).

[11] C. R. Jacob and M. Reiher, The Journal of Chemical Physics **130**, 084106 (2009).

[12] X. Cheng and R. P. Steele, The Journal of Chemical Physics **141**, 104105 (2014).

[13] C. R. Jacob, S. Luber, and M. Reiher, The Journal of Physical Chemistry B **113**, 6558 (2009).

[14] M. W. D. Hanson-Heine, The Journal of Chemical Physics **143**, 164104 (2015).

[15] T. C. Thompson and D. G. Truhlar, The Journal of Chemical Physics **77**, 3031 (1982).

[16] K. Yagi, M. Keçeli, and S. Hirata, The Journal of Chemical Physics **137**, 204118 (2012).

[17] R. Johnson, Nist 101. computational chemistry comparison and benchmark database (1999).

[18] S. Carter, J. M. Bowman, and N. C. Handy, Theoretical Chemistry Accounts: Theory, Computation, and Modeling (Theoretica Chimica Acta) **100**, 191 (1998).

doi:10.6342/NTU202201978

[19] J. Pipek and P. G. Mezey, The Journal of Chemical Physics **90**, 4916 (1989).

[20] J. M. Foster and S. F. Boys, Reviews of Modern Physics **32**, 300 (1960).

[21] S. F. Boys, Reviews of Modern Physics **32**, 296 (1960).

[22] C. Edmiston and K. Ruedenberg, Reviews of Modern Physics **35**, 457 (1963).

[23] M. W. D. Hanson-Heine, The Journal of Chemical Physics **144**, 204116 (2016).

[24] A. Molina, P. Smereka, and P. M. Zimmerman, The Journal of Chemical Physics **144**, 124111 (2016).

[25] P. M. Zimmerman and P. Smereka, Journal of Chemical Theory and Computation **12**, 1883 (2016).

[26] B. Thomsen, K. Yagi, and O. Christiansen, Chemical Physics Letters **610-611**, 288 (2014).

[27] K. Yagi, P.-C. Li, K. Shirota, T. Kobayashi, and Y. Sugita, Physical Chemistry Chemical Physics **17**, 29113 (2015).

[28] K. Yagi, H. Otaki, P. Li, B. Thomsen, and Y. Sugita, Weight averaged anharmonic vibrational calculations: Applications to polypeptide, lipid bilayers, and polymer materials (2019).

[29] K. Yagi, S. Re, T. Mori, and Y. Sugita, Current Opinion in Structural Biology **72**, 88 (2022).

[30] K. Yagi and Y. Sugita, Journal of Chemical Theory and Computation **17**, 5007 (2021).

doi:10.6342/NTU202201978

[31] M. J. Frisch, G. W. Trucks, H. B. Schlegel, G. E. Scuseria, M. A. Robb, J. R. Cheeseman, G. Scalmani, V. Barone, G. A. Petersson, H. Nakatsuji, X. Li, M. Caricato, A. V. Marenich, J. Bloino, B. G. Janesko, R. Gomperts, B. Mennucci, H. P. Hratchian, J. V. Ortiz, A. F. Izmaylov, J. L. Sonnenberg, D. Williams-Young, F. Ding, F. Lipparini, F. Egidi, J. Goings, B. Peng, A. Petrone, T. Henderson, D. Ranasinghe, V. G. Zakrzewski, J. Gao, N. Rega, G. Zheng, W. Liang, M. Hada, M. Ehara, K. Toyota, R. Fukuda, J. Hasegawa, M. Ishida, T. Nakajima, Y. Honda, O. Kitao, H. Nakai, T. Vreven, K. Throssell, J. A. Montgomery, Jr., J. E. Peralta, F. Ogliaro, M. J. Bearpark, J. J. Heyd, E. N. Brothers, K. N. Kudin, V. N. Staroverov, T. A. Keith, R. Kobayashi, J. Normand, K. Raghavachari, A. P. Rendell, J. C. Burant, S. S. Iyengar, J. Tomasi, M. Cossi, J. M. Millam, M. Klene, C. Adamo, R. Cammi, J. W. Ochterski, R. L. Martin, K. Morokuma, O. Farkas, J. B. Foresman, and D. J. Fox, Gaussian˜16 Revision B.01 (2016), gaussian Inc. Wallingford CT.

[32] Q.-R. Huang, T. Nishigori, M. Katada, A. Fujii, and J.-L. Kuo, Physical Chemistry Chemical Physics **20**, 13836 (2018).

[33] K.-L. Ho, L.-Y. Lee, M. Katada, A. Fujii, and J.-L. Kuo, Physical Chemistry Chemical Physics **18**, 30498 (2016).

[34] R. B. Lehoucq, D. C. Sorensen, and C. Yang, in *Software, environments, tools* (1998).

[35] X. Cheng, J. J. Talbot, and R. P. Steele, The Journal of Chemical Physics **145**, 124112 (2016).

doi:10.6342/NTU202201978

[36] E. G. Buchanan, J. C. Dean, T. S. Zwier, and E. L. Sibert, The Journal of Chemical Physics **138**, 064308 (2013).

[37] E. L. Sibert, D. P. Tabor, N. M. Kidwell, J. C. Dean, and T. S. Zwier, The Journal of Physical Chemistry A **118**, 11272 (2014).

[38] E. L. Sibert, N. M. Kidwell, and T. S. Zwier, The Journal of Physical Chemistry B **118**, 8236 (2014).

[39] C. T. Wolke, J. A. Fournier, L. C. Dzugan, M. R. Fagiani, T. T. Odbadrakh, H. Knorke, K. D. Jordan, A. B. McCoy, K. R. Asmis, and M. A. Johnson, Science **354**, 1131 (2016).

[40] Q.-R. Huang, Y.-C. Li, K.-L. Ho, and J.-L. Kuo, Physical Chemistry Chemical Physics **20**, 7653 (2018).

[41] R. Dennington, T. A. Keith, and J. M. Millam, Gaussview Version 6 (2019), semichem Inc. Shawnee Mission KS.

doi:10.6342/NTU202201978

doi:10.6342/NTU202201978

Appendix A — Visualization of the vibrational modes

In this appendix, the visualization of the modes using GaussView 6 [41] are shown.

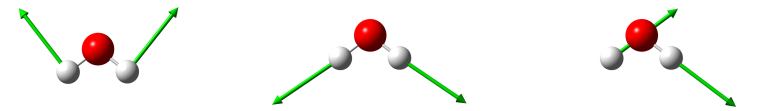

(a) NC 1: 1622 (b) NC 2: 3803 (c) NC 3: 3937

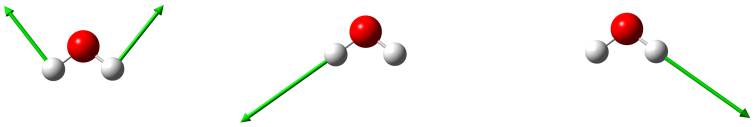

(d) OC 1: 1622 (e) OC 2: 3870 (f) OC 3: 3870

Figure A.1: The frequencies and vibrational vectors of water monomer in NC and OC. The frequencies are shown in cm^{-1}.

doi:10.6342/NTU202201978

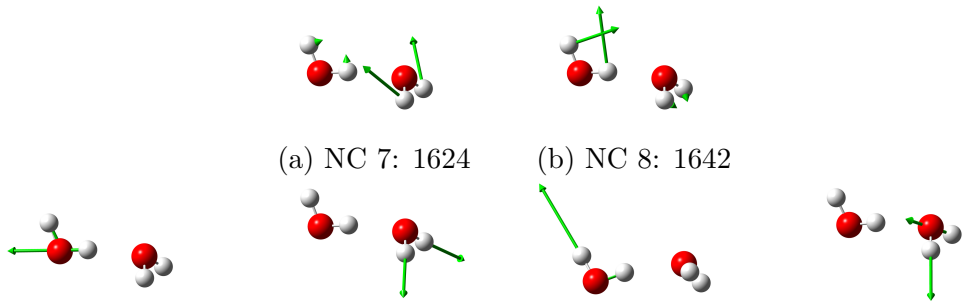

(a) NC 7: 1624 (b) NC 8: 1642

(c) NC 9: 3704 (d) NC 10: 3795 (e) NC 11: 3904 (f) NC 12: 3924

Figure A.2: The frequencies and vibrational vectors of water dimer in NC. The frequencies are shown in cm^{-1}.

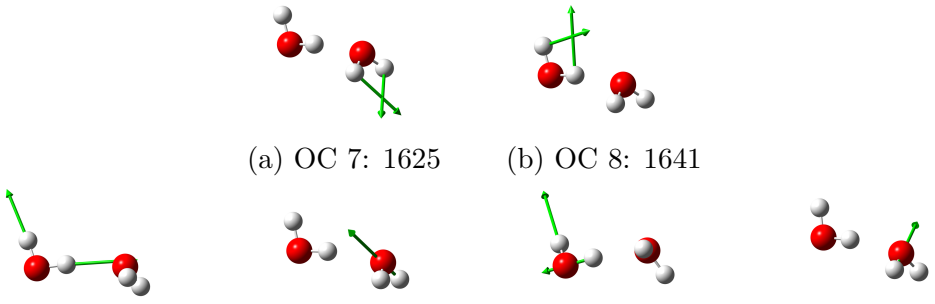

(a) OC 7: 1625 (b) OC 8: 1641

(c) OC 9: 3725 (d) OC 10: 3860 (e) OC 11: 3884 (f) OC 12: 3860

Figure A.3: The frequencies and vibrational vectors of water dimer in OC. The frequencies are shown in cm^{-1}.

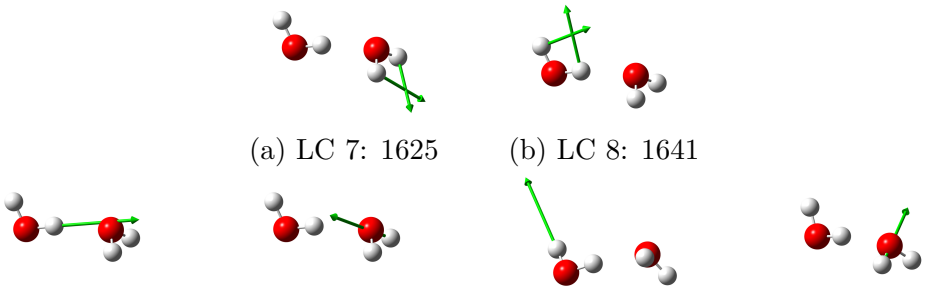

(a) LC 7: 1625 (b) LC 8: 1641

(c) LC 9: 3727 (d) LC 10: 3860 (e) LC 11: 3882 (f) LC 12: 3860

Figure A.4: The frequencies and vibrational vectors of water dimer in LC. The frequencies are shown in cm^{-1}.

doi:10.6342/NTU202201978

(a) NC 9: 1641 (b) NC 10: 1649 (c) NC 11: 1654 (d) NC 12: 1673

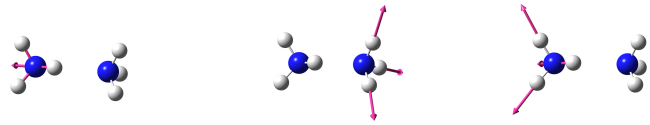

(e) NC 13: 3446 (f) NC 14: 3476 (g) NC 15: 3596

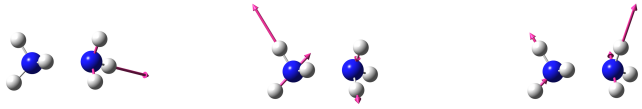

(h) NC 16: 3628 (i) NC 17: 3632 (j) NC 18: 3632

Figure A.5: The frequencies and vibrational vectors of ammonia dimer in NC. The frequencies are shown in cm^{-1}.

(a) LNM 9: 1647 (b) LNM 10: 1677 (c) LNM 11: 1647 (d) LNM 12: 1677

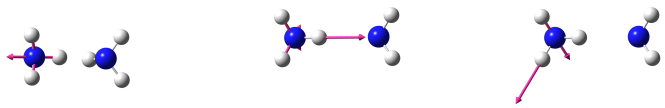

(e) LNM 13: 3415 (f) LNM 14: 3577 (g) LNM 15: 3629

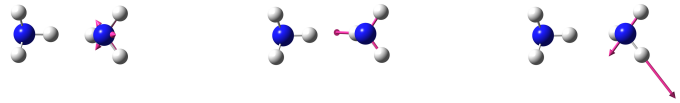

(h) LNM 16: 3415 (i) LNM 17: 3577 (j) LNM 18: 3629

Figure A.6: The frequencies and vibrational vectors of ammonia dimer in LNM. The frequencies are shown in cm^{-1}.

doi:10.6342/NTU202201978

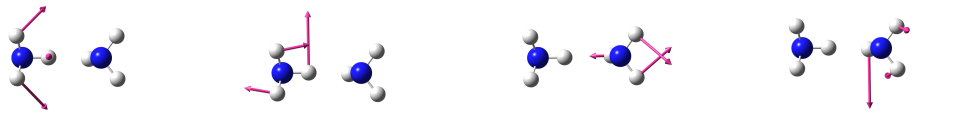

(a) LC 9: 1647 (b) LC 10: 1673 (c) LC 11: 1648 (d) LC 12: 1650

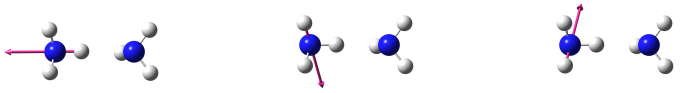

(e) LC 13: 3514 (f) LC 14: 3582 (g) LC 15: 3582

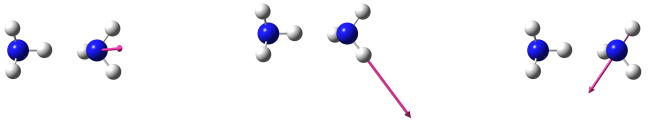

(h) LC 16: 3575 (i) LC 14: 3582 (j) LC 16: 3582

Figure A.7: The frequencies and vibrational vectors of ammonia dimer in LC. The frequencies are shown in cm^{-1}.

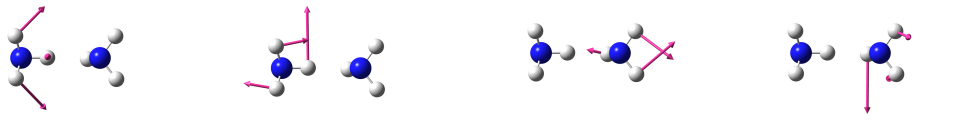

(a) OC 9: 1648 (b) OC 10: 1673 (c) OC 11: 1648 (d) OC 12: 1650

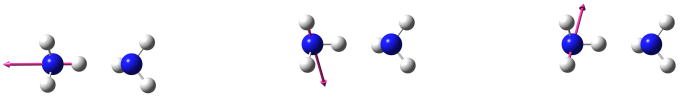

(e) OC 13: 3513 (f) OC 14: 3582 (g) OC 15: 3582

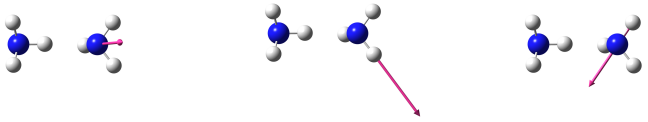

(h) OC 16: 3575 (i) OC 17: 3582 (j) OC 18: 3582

Figure A.8: The frequencies and vibrational vectors of ammonia dimer in OC. The frequencies are shown in cm^{-1}.

doi:10.6342/NTU202201978

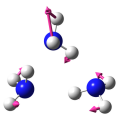

(a) NC 16: 1639

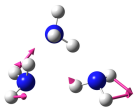

(b) NC 17: 1639

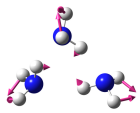

(c) NC 18: 1664

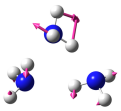

(d) NC 19: 1677

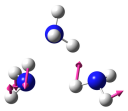

(e) NC 20: 1677

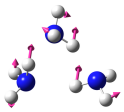

(f) NC 21: 1680

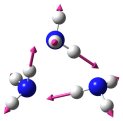

(g) NC 22: 3404

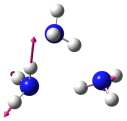

(h) NC 23: 3420

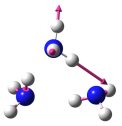

(i) NC 24: 3420

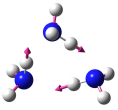

(j) NC 25: 3574

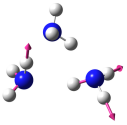

(k) NC 26: 3578

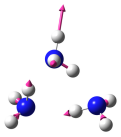

(l) NC 27: 3578

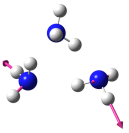

(m) NC 28: 3628

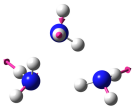

(n) NC 29: 3628

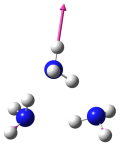

(o) NC 30: 3629

Figure A.9: The frequencies and vibrational vectors of ammonia trimer in NC. The frequencies are shown in cm^{-1}.

doi:10.6342/NTU202201978

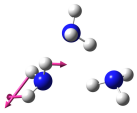

(a) LNM 16: 1647

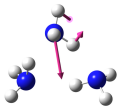

(b) LNM 17: 1647

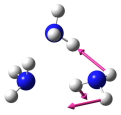

(c) LNM 18: 1647

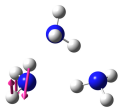

(d) LNM 19: 1677

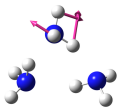

(e) LNM 20: 1677

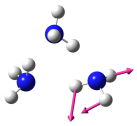

(f) LNM 21: 1677

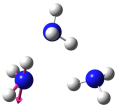

(g) LNM 22: 3415

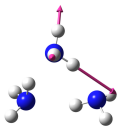

(h) LNM 23: 3415

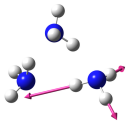

(i) LNM 24: 3415

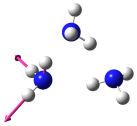

(j) LNM 25: 3577

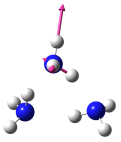

(k) LNM 26: 3577

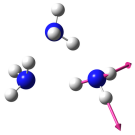

(l) LNM 27: 3577

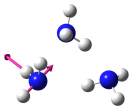

(m) LNM 28: 3628

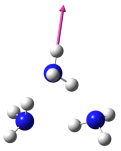

(n) LNM 29: 3628

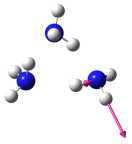

(o) LNM 30: 3628

Figure A.10: The frequencies and vibrational vectors of ammonia trimer in LNM. The frequencies are shown in cm^{-1}.

doi:10.6342/NTU202201978

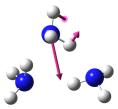

(a) LC 16: 1647

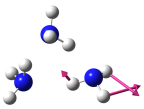

(b) LC 17: 1647

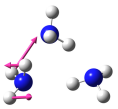

(c) LC 18: 1647

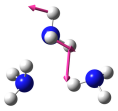

(d) LC 19: 1677

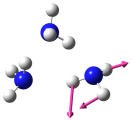

(e) LC 20: 1677

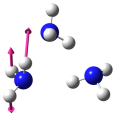

(f) LC 21: 1677

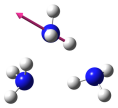

(g) LC 22: 3462

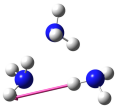

(h) LC 23: 3462

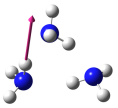

(i) LC 24: 3462

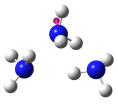

(j) LC 25: 3579

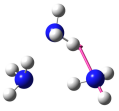

(k) LC 26: 3579

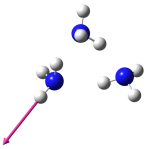

(l) LC 27: 3579

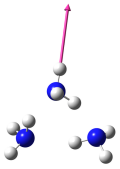

(m) LC 28: 3579

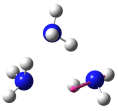

(n) LC 39: 3579

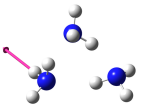

(o) LC 30: 3579

Figure A.11: The frequencies and vibrational vectors of ammonia trimer in LC. The frequencies are shown in cm^{-1}.

doi:10.6342/NTU202201978

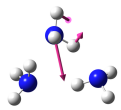

(a) OC 16: 1647

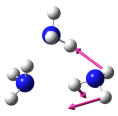

(b) OC 17: 1647

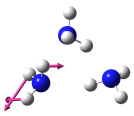

(c) OC 18: 1647

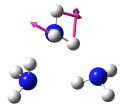

(d) OC 19: 1677

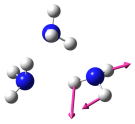

(e) OC 20: 1677

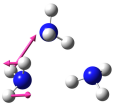

(f) OC 21: 1677

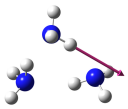

(g) OC 22: 3462

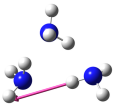

(h) OC 23: 3462

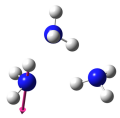

(i) OC 24: 3462

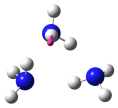

(j) OC 25: 3579

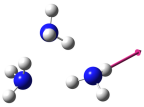

(k) OC 26: 3579

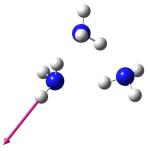

(l) OC 27: 3579

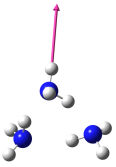

(m) OC 28: 3579

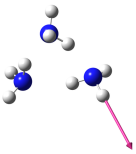

(n) OC 29: 3579

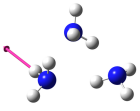

(o) OC 30: 3579

Figure A.12: The frequencies and vibrational vectors of ammonia trimer in OC. The frequencies are shown in cm^{-1}.

doi:10.6342/NTU202201978

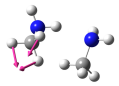

(a) NC 19: 1438

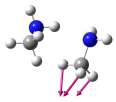

(b) NC 20: 1444

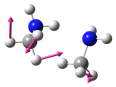

(c) NC 21: 1492

(d) NC 22: 1500

(e) NC 23: 1512

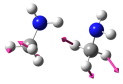

(f) NC 24: 1518

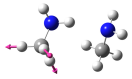

(g) NC 27: 3025

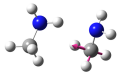

(h) NC 28: 3046

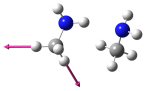

(i) NC 29: 3116

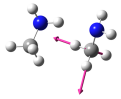

(j) NC 30: 3133

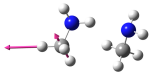

(k) NC 31: 3157

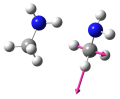

(l) NC 32: 3171

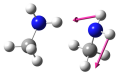

(m) NC 25: 1641

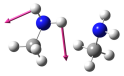

(n) NC 26: 1669

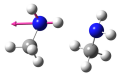

(o) NC 33: 3456

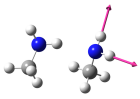

(p) NC 34: 3507

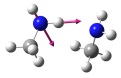

(q) NC 35: 3582

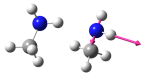

(r) NC 36: 3605

Figure A.13: The frequencies and vibrational vectors of methylamine dimer in NC. The frequencies are shown in cm^{-1}.

doi:10.6342/NTU202201978

(a) LNM 19: 1439

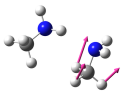

(b) LNM 20: 1444

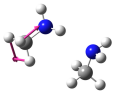

(c) LNM 21: 1493

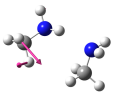

(d) LNM 22: 1513

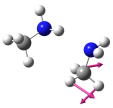

(e) LNM 23: 1499

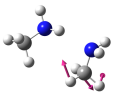

(f) LNM 24: 1516

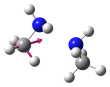

(g) LNM 27: 3025

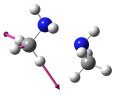

(h) LNM 28: 3116

(i) LNM 29: 3156

(j) LNM 30: 3045

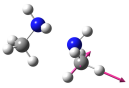

(k) LNM 31: 3133

(l) LNM 32: 3170

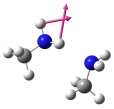

(m) LNM 25: 1669

(n) LNM 26: 1642

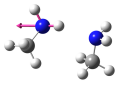

(o) LNM 33: 3456

(p) LNM 34: 3582

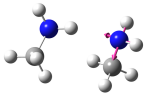

(q) LNM 35: 3507

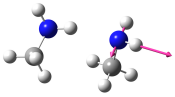

(r) LNM 36: 3604

Figure A.14: The frequencies and vibrational vectors of methylamine dimer in LNM. The frequencies are shown in cm^{-1}.

doi:10.6342/NTU202201978

(a) LC 19: 1438

(b) LC 20: 1444

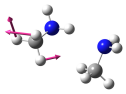

(c) LC 21: 1501

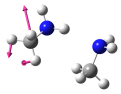

(d) LC 22: 1504

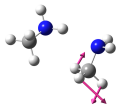

(e) LC 23: 1506

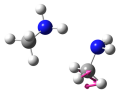

(f) LC 24: 1510

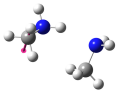

(g) LC 27: 3044

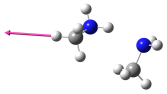

(h) LC 28: 3128

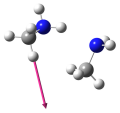

(i) LC 29: 3127

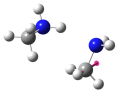

(j) LC 30: 3136

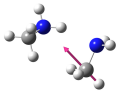

(k) LC 31: 3072

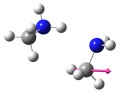

(l) LC 32: 3142

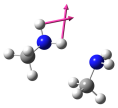

(m) LC 25: 1669

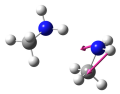

(n) LC 26: 1642

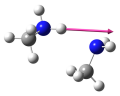

(o) LC 33: 3481

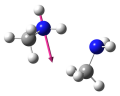

(p) LC 34: 3558

(q) LC 35: 3560

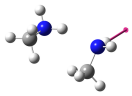

(r) LC 36: 3553

Figure A.15: The frequencies and vibrational vectors of methylamine dimer in LC. The frequencies are shown in cm^{-1}.

doi:10.6342/NTU202201978

(a) OC 19: 1438

(b) OC 20: 1444

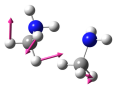

(c) OC 21: 1502

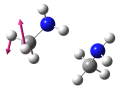

(d) OC 22: 1504

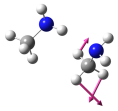

(e) OC 23: 1506

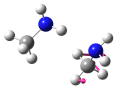

(f) OC 24: 1510

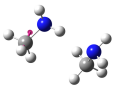

(g) OC 27: 3044

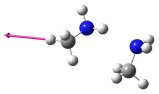

(h) OC 28: 3128

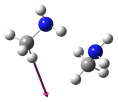

(i) OC 29: 3127

(j) OC 30: 3136

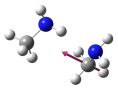

(k) OC 31: 3072

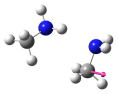

(l) OC 32: 3142

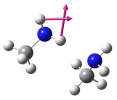

(m) OC 25: 1669

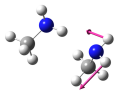

(n) OC 26: 1642

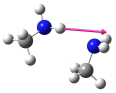

(o) OC 33: 3481

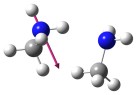

(p) OC 34: 3558

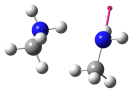

(q) OC 35: 3554

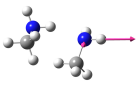

(r) OC 36: 3559

Figure A.16: The frequencies and vibrational vectors of methylamine dimer in OC. The frequencies are shown in cm^{-1}.

doi:10.6342/NTU202201978

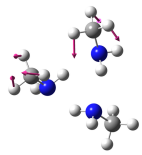

(a) NC 31: 1436

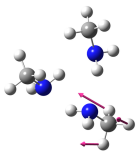

(b) NC 32: 1438

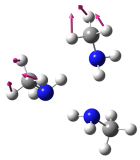

(c) NC 33: 1442

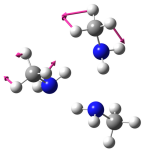

(d) NC 34: 1491

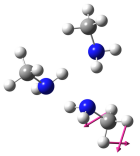

(e) NC 35: 1492

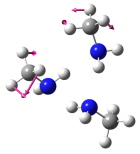

(f) NC 36: 1497

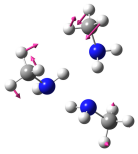

(g) NC 37: 1512

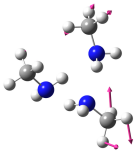

(h) NC 38: 1516

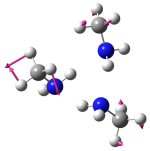

(i) NC 39: 1518

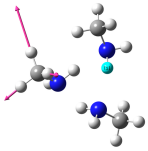

(j) NC 43: 3031

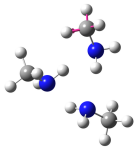

(k) NC 44: 3035

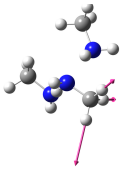

(l) NC 45: 3037

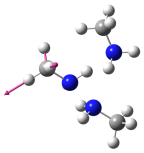

(m) NC 46: 3115

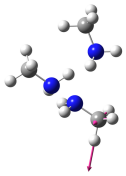

(n) NC 47: 3119

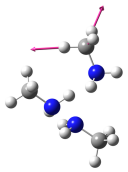

(o) NC 48: 3121

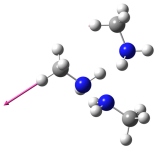

(p) NC 49: 3153

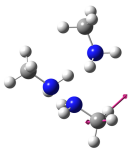

(q) NC 50: 3155

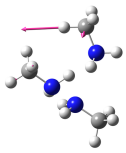

(r) NC 51: 3160

Figure A.17: The frequencies and vibrational vectors of the methyl groups of methylamine trimer in NC. The frequencies are shown in cm^{-1}.

doi:10.6342/NTU202201978

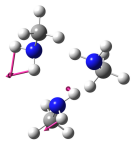

(a) NC 40: 1649

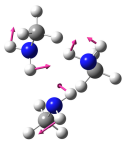

(b) NC 41: 1657

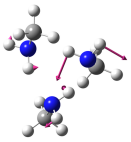

(c) NC 42: 1673

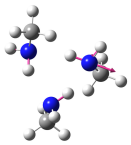

(d) NC 52: 3405

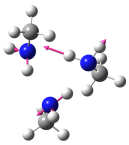

(e) NC 53: 3426

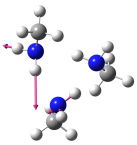

(f) NC 54: 3433

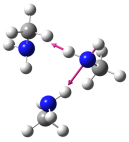

(g) NC 55: 3570

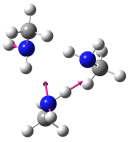

(h) NC 56: 3578

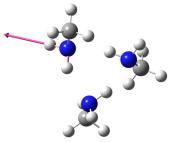

(i) NC 27: 3580

Figure A.18: The frequencies and vibrational vectors of the amino groups of methylamine trimer in NC. The frequencies are shown in cm^{-1}.

doi:10.6342/NTU202201978

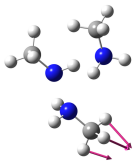

(a) LNM 31: 1438

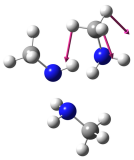

(b) LNM 32: 1439

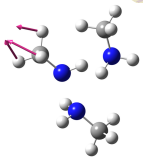

(c) LNM 33: 1438

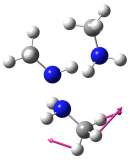

(d) LNM 34: 1493

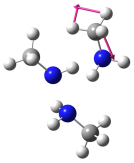

(e) LNM 35: 1493

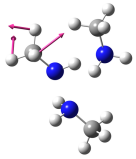

(f) LNM 36: 1493

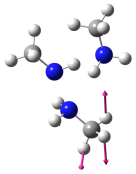

(g) LNM 37: 1516

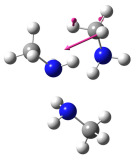

(h) LNM 38: 1514

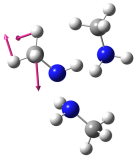

(i) LNM 39: 1516

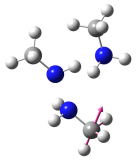

(j) LNM 43: 3037

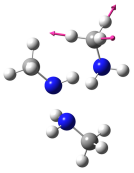

(k) LNM 44: 3035

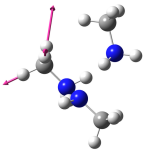

(l) LNM 45: 3031

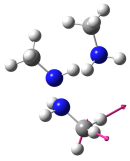

(m) LNM 46: 3119

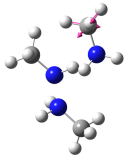

(n) LNM 47: 3121

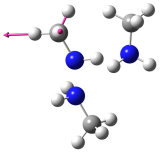

(o) LNM 48: 3115

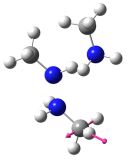

(p) LNM 49: 3155

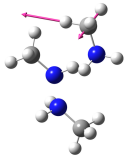

(q) LNM 50: 3160

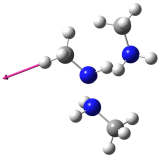

(r) LNM 51: 3153

Figure A.19: The frequencies and vibrational vectors of the methyl groups of methylamine trimer in LNM. The frequencies are shown in cm^{-1}.

doi:10.6342/NTU202201978

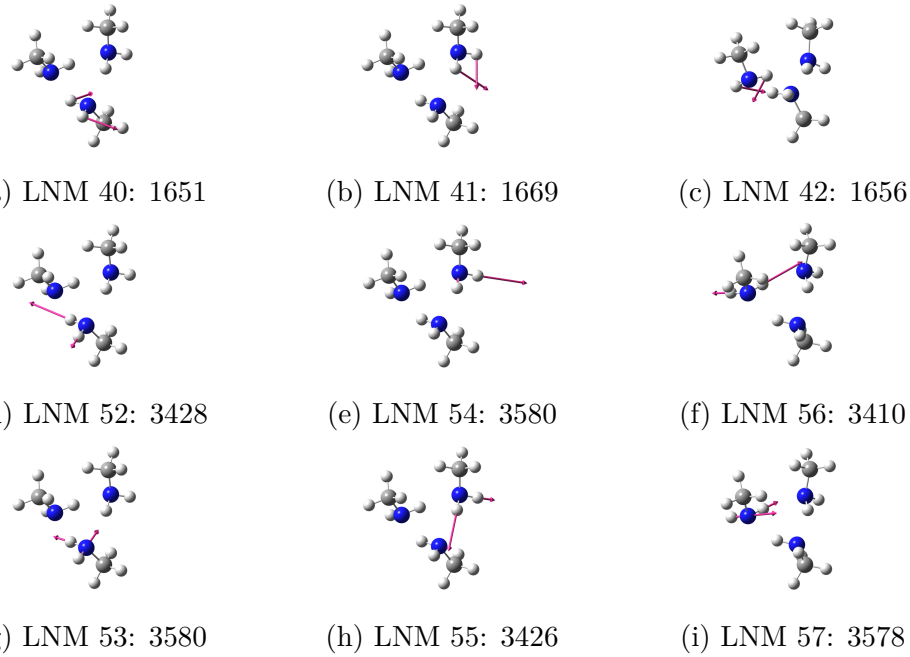

(a) LNM 40: 1651 (b) LNM 41: 1669 (c) LNM 42: 1656

(d) LNM 52: 3428 (e) LNM 54: 3580 (f) LNM 56: 3410

(g) LNM 53: 3580 (h) LNM 55: 3426 (i) LNM 57: 3578

Figure A.20: The frequencies and vibrational vectors of the amino groups of methylamine trimer in LNM. The frequencies are shown in cm^{-1}.

doi:10.6342/NTU202201978

(a) LC 31: 1439

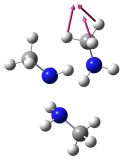

(b) LC 32: 1438

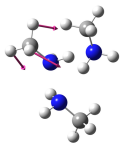

(c) LC 33: 1438

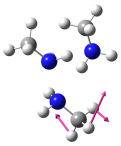

(d) LC 34: 1504

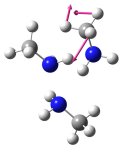

(e) LC 35: 1503

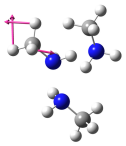

(f) LC 36: 1503

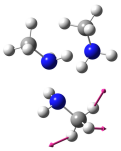

(g) LC 37: 1506

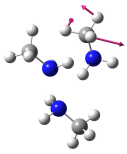

(h) LC 38: 1504

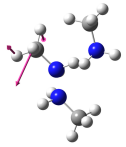

(i) LC 39: 1509

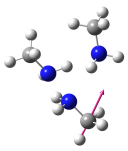

(j) LC 43: 3062

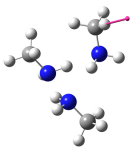

(k) LC 44: 3057

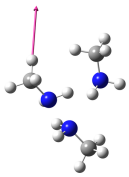

(l) LC 45: 3055

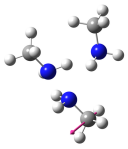

(m) LC 46: 3125

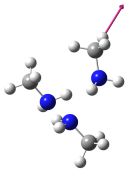

(n) LC 47: 3127

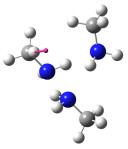

(o) LC 48: 3117

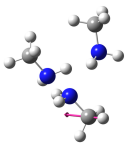

(p) LC 49: 3125

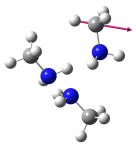

(q) LC 50: 3132

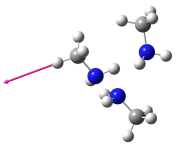

(r) LC 51: 3128

Figure A.21: The frequencies and vibrational vectors of the methyl groups of methylamine trimer in LC. The frequencies are shown in cm^{-1}.

doi:10.6342/NTU202201978

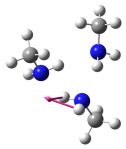

(a) LC 40: 1653

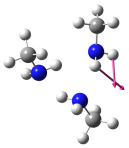

(b) LC 41: 1670

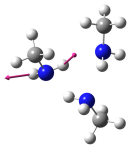

(c) LC 42: 1657

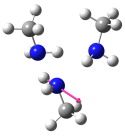

(d) LC 52: 3449

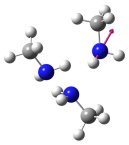

(e) LC 53: 3429

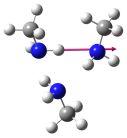

(f) LC 54: 3447

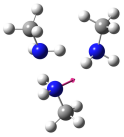

(g) LC 55: 3558

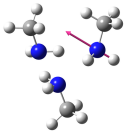

(h) LC 56: 3552

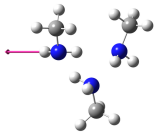

(i) LC 57: 3558

Figure A.22: The frequencies and vibrational vectors of the amino groups of methylamine trimer in LC. The frequencies are shown in cm^{-1}.

doi:10.6342/NTU202201978

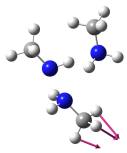

(a) OC 31: 1438

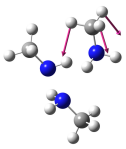

(b) OC 32: 1439

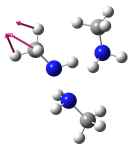

(c) OC 33: 1439

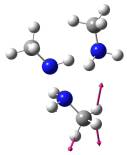

(d) OC 34: 1505

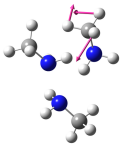

(e) OC 35: 1504

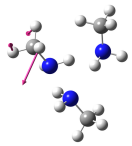

(f) OC 36: 1504

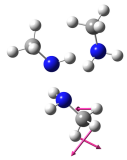

(g) OC 37: 1504

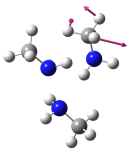

(h) OC 38: 1503

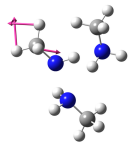

(i) OC 39: 1508

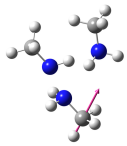

(j) OC 43: 3062

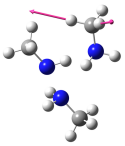

(k) OC 44: 3099

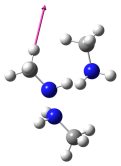

(l) OC 45: 3071

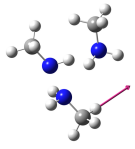

(m) OC 46: 3124

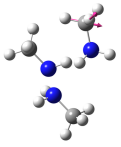

(n) OC 47: 3090

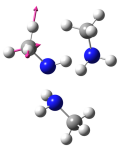

(o) OC 48: 3112

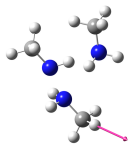

(p) OC 49: 3124

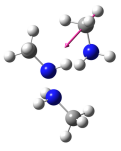

(q) OC 50: 3127

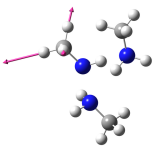

(r) OC 51: 3116

Figure A.23: The frequencies and vibrational vectors of the methyl groups of methylamine trimer in OC. The frequencies are shown in cm^{-1}.

doi:10.6342/NTU202201978

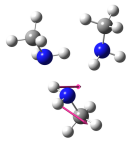

(a) OC 40: 1651

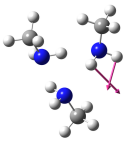

(b) OC 41: 1669

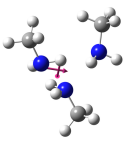

(c) OC 42: 1656

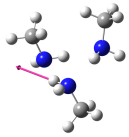

(d) OC 52: 3449

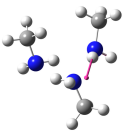

(e) OC 53: 3428

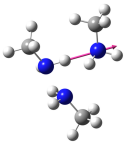

(f) OC 54: 3446

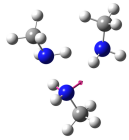

(g) OC 55: 3558

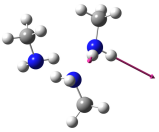

(h) OC 56: 3551

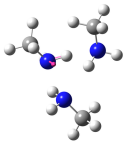

(i) OC 57: 3558

Figure A.24: The frequencies and vibrational vectors of the amino groups of methylamine trimer in OC. The frequencies are shown in cm^{-1}.

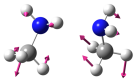

(a) NC 15: 1180

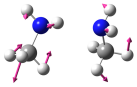

(b) NC 16: 1180

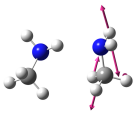

(c) NC 17: 1342

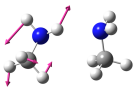

(d) NC 18: 1367

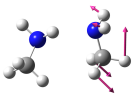

(e) LNM 15: 1180

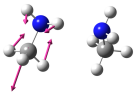

(f) LNM 16: 1180

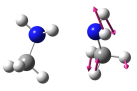

(g) LNM 17: 1342

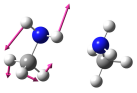

(h) LNM 18: 1367

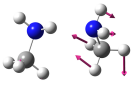

(i) OC 15: 1180

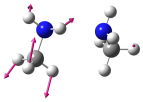

(j) OC 16: 1180

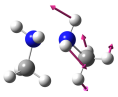

(k) OC 17: 1342

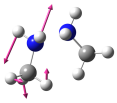

(l) OC 18: 1367

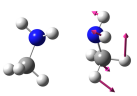

(m) LC 15: 1184

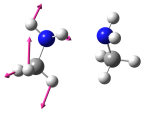

(n) LC 16: 1207

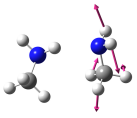

(o) LC 17: 1343

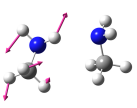

(p) LC 18: 1339

Figure A.25: The frequencies and vibrational vectors of the rocking motions of methylamine dimer in NC, LNM, OC and LC. The frequencies are shown in cm^{-1}.

doi:10.6342/NTU202201978

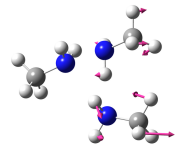

(a) NC 25: 1185

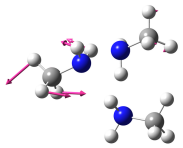

(b) NC 26: 1187

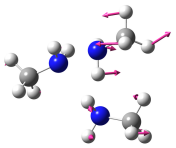

(c) NC 27: 1189

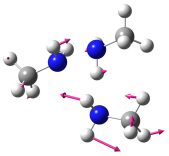

(d) NC 28: 1362

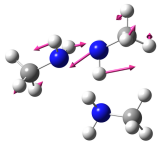

(e) NC 29: 1367

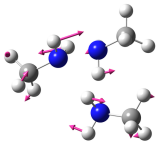

(f) NC 30: 1372

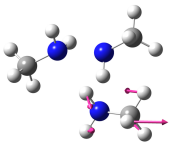

(g) OC 25: 1186

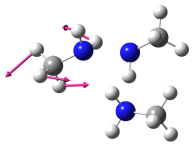

(h) OC 26: 1187

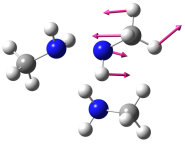

(i) OC 27: 1188

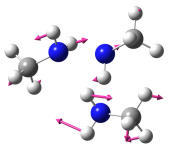

(j) OC 28: 1362

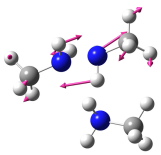

(k) OC 29: 1367

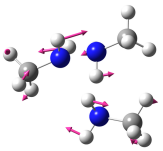

(l) OC 30: 1371

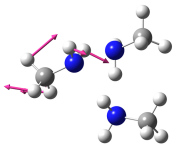

(m) LNM 25: 1187

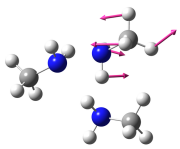

(n) LNM 26: 1187

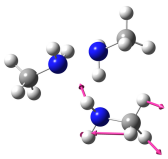

(o) LNM 27: 1185

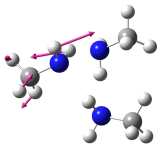

(p) LNM 28: 1369

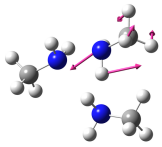

(q) LNM 29: 1369

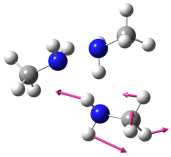

(r) LNM 30: 1365

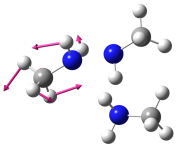

(s) LC 25: 1232

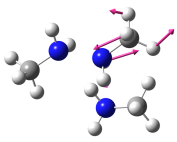

(t) LC 26: 1232

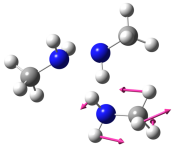

(u) LC 27: 1244

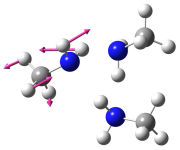

(v) LC 28: 1328

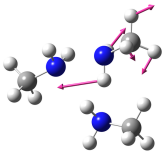

(w) LC 29: 1328

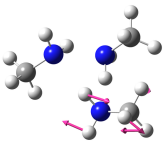

(x) LC 30: 1313

Figure A.26: The frequencies and vibrational vectors of the rocking motions of methylamine trimer in NC, OC, LNM and LC. The frequencies are shown in cm^{-1}.

doi:10.6342/NTU202201978